Potassium fertilizer via hydrothermal alteration of K-feldspar ore

Citation: Ciceri, Davide, Marcelo de Oliveira, and Antoine Allanore. "Potassium Fertilizer via Hydrothermal Alteration of K-Feldspar Ore." Green Chem. 19, 21 (September 2017): 5187–5202

As Published: http://dx.doi.org/ 10.1039/C7GC02633A

Publisher: Royal Society of Chemistry

Persistent URL: http://hdl.handle.net/1721.1/114764

Version: Author's final manuscript: final author's manuscript post peer review, without publisher's formatting or copy editing

GREEN-CHEMISTRY SYNTHESIS OF POTASSIUM FERTILIZER VIA HYDROTHERMAL ALTERATION OF K-FELDSPAR ORE

Davide Ciceri, Marcelo de Oliveira, Antoine Allanore

ABSTRACT

Fertilizers ensure the necessary agricultural yields to feed an increasing world population. Augmenting fertilizer use conflicts with environmental concerns such as eutrophication and soil pollution, as well as with limited availability of fertilizers in the Global South. Currently, potassium fertilizers are soluble salts such as KCl, which are mined in the northern hemisphere. Two key issues arise for tropical agriculture. First, the inherent solubility of potassium salts questions their efficacy in weathered soils. Second, long-distance transportation leaves unsolved the problems of limited local supplies and infrastructure, freight-related CO_2 emissions and cost of the fertilizer for the end user. In this work, we synthesize according to green-chemistry principles a novel potassium-bearing material which mineralogy and elemental release have the potential to overcome the limitations of KCl. We process in mild hydrothermal conditions (T=200 °C; P~14 atm; t=5 h) locally available K-feldspar ore (ultrapotassic syenite) and CaO. The resulting hydrothermal material is characterized using X-Ray Diffraction (XRD), Electron Microscopy (EM), Electron Probe Micro-Analyzer (EPMA), Particle Size Distribution (PSD) and Specific Surface Area (SSA). Additionally, leaching tests are performed, showing that the availability of potassium in the processed material is two orders of magnitude higher than in the raw K-feldspar ore. This work introduces a green-chemistry paradigm for the synthesis of potassium fertilizers.

Keywords: fertilizers, K-feldspar, hydrothermal chemistry, potash, ultrapotassic syenite.

1. INTRODUCTION

To address global food security concerns, agricultural yields need to increase substantially. Improving agriculture in the tropical region is driven by the projection that this part of the planet will host half of the world population by 2050[1]. Fertilizers are necessary for such an improvement, sustaining a productive agriculture and providing nutritious food[2-5]. This work focuses on potassium fertilizers or potash (Table 1).

Currently, despite regional soil variations one type of potassium fertilizer, *i.e.* KCl, dominates the global market[5]. KCl is mined in the northern hemisphere, far from the tropical belt. The distance between the producers and the end users is directly proportional to CO_2 emissions due to transport (ESI 1), and determines the cost of the fertilizer. As a significant example, on March 31st 2017 the price of potash was 339 US$ ton$^{-1}_{K2O}$ F.O.B in Vancouver, Canada, and 575 US$ ton$^{-1}_{K2O}$ at the farmer's gate in the Cerrado region of Brazil. In addition to cost, properties of tropical soils such as low pH, high oxides content and limited Cation-Exchange Capacity (CEC) suggest that KCl may not be appropriate for tropical agriculture[6,7]. Ionic fertilizers are not efficient, and high leaching losses have been reported, in extreme cases as high as 35-60%[8–11]. Potassium management has not been a priority of tropical agriculture, and

very limited specific information has been made available regarding possible undesired effects of KCl on the total environment in either hemisphere's agricultural environment. Underground mining of KCl is reported to expose miners to a higher incidence of bronchitis and lung dysfunctions[12], and KCl fertilization may be linked to increased Cd uptake by plants as well as increased cardiovascular diseases and obesity[13]. Furthermore, KCl is not always allowed in organic agriculture, is discouraged in hydroponic cultivations and is not tolerated by certain crops due to chloride ions, which may also affect soil microbial communities[5,13–16]. Overall, increasing agricultural yields in the tropics remains challenging because rapid population growth is occurring, but the fertility of nutrient-depleted soils is not being improved commensurately, due to major economic barriers, and/or limited soil benefits of existing potassium fertilizers. This is reflected in the regional potential balance of K_2O, that according to data from the Food and Agriculture Organization (FAO) will be negative in most areas of the world for the cumulative period 2016-2019[17].

An alternative to KCl worth considering to improve the availability of potash supplies in tropical agriculture is the mineral K-feldspar ($KAlSi_3O_8$). K-feldspar constitutes approximately 60% of the world's potential K resources. In igneous rocks, K-feldspar occurs as the largest constituent of granitoids. However, higher concentrations of K-feldspar (>70 wt%) occur only in two types of ores, *i.e.* syenites (plutonic) and trachytes (volcanic). Ultrapotassic syenites are benign, abundant, and evenly distributed raw materials[18]. They are mined at the Earth's surface, simplifying industrial logistics and reduce capital cost with respect to solution or underground mining used for KCl extraction (Table 1). As an example, K-feldspar processing for direct powder application (stonemeal) requires only mechanical operations such as comminution and sieving, eliminating the need for water and relatively complex recrystallization units which are necessary for refining sylvinite ore[5,18,19]. The average potassium content in ultrapotassic syenites is equivalent to ~13 wt% K_2O[18], which is comparable to that of unprocessed sylvinite ores in Canada (Table 1). However, ultrapotassic syenites carry other beneficial elements to crops, which include ~63 wt % of SiO_2 and ~5 wt % of micronutrients such as Ca and Mg from varietal mafic minerals. A possible drawback for fertilization purposes is given by ~17 wt % of Al_2O_3, which, however, is already present at relatively high concentrations in tropical soils, in the form of very stable and plant-unavailable oxides. Despite such advantages, K-feldspar and other framework alumino-silicates have been traditionally considered an ineffective source of macro-nutrients due to their slow dissolution rate[4,18,20].

A paradigm shift towards alternative potash sources such as K-feldspar requires the development of green and cost-effective processes that enhance the availability of potassium ions from the feldspar's alumino-silicate framework. Engineering such processes requires a simultaneous consideration of the chemical behavior of the K_2O, Al_2O_3, and SiO_2 components of the feldspar, and assign to each of such components

a specific soil-related function in the processed material. Several laboratory-scale approaches have been proposed in that direction including i) direct soil application of comminuted and/or mechano-activated K-feldspar[3,4,18,20,21], and exploitation of microorganism-mediated dissolution[10,22] (bioweathering) ii) alkaline hydrothermal alteration[23–27] and iii) calcination in presence of fluxes[3,28–30]. Alkaline hydrothermal alteration of K-feldspar ores is particularly appealing, due to relatively low processing temperatures (150°C-250°C) and virtually zero waste. The fields of ceramic, cement and geopolymer-concrete science have provided insights into the hydrothermal reactivity of alumino-silicate resources (Table ESI 1)[31–34], and authors from Chinese schools have recently reported on K-feldspar processing[24–27,35]. Despite such progress, current knowledge regarding the hydrothermal alteration of K-feldspar is very limited[23]. Furthermore, for widespread adoption of materials alternative to KCl, the development of a proper processing route must consider soil science and economic principles. As an example, expensive and/or excessive use of alkali sources and prolonged processing times reported in the literature thus far result in the three-fold problem of formation of soluble potassium species that can be leached away quickly, formation of waste or byproducts, and high processing and environmental costs that are often not competitive with KCl[24-30].

We have critically evaluated K-feldspar ores elsewhere, and provided a correlation between their petrographic features and elemental leaching[18]. As the next step, here we present a material obtained by processing in mild hydrothermal conditions (200 °C, ~14 atm, 5 h, m_{solid}:m_{H2O}=0.25) a mixture obtained by jointly milling $Ca(OH)_2$ (14.9 wt %) and ultrapotassic syenite (85.1 wt%; equivalent to 80.4 wt% of K-feldspar or 12.2 wt% of K_2O in the unprocessed feed mixture). The dried material, herein referred to as the *hydrothermal material*, is characterized by X-Ray Powder Diffraction (XRD), Scanning Electron Microscopy (SEM), Electron Probe Micro-Analyzer (EPMA), Particle Size Distribution (PSD) analysis, Specific Surface Area according to the BET method (BET-SSA) and batch leaching tests. We identify and quantify the mineral phases composing the hydrothermal material as well as their degree of elemental incorporations with respect to stoichiometric chemical formulae. We discover that the feldspar framework undergoes structural and chemical changes, a phenomenon we term alteration. In the leaching test, the potassium released from the hydrothermal material after 24 h is shown to be two orders of magnitude higher than in the corresponding raw material. The overall discussion is framed according to the overarching goal: engineer a green-chemistry process scalable to industrial outputs that can truly benefit tropical soils. A rigorous analysis of the hydrothermal material provides new insights on Ca-mediated hydrothermal alteration of K-feldspar, bridging materials science and processing technology for their application in agriculture.

Table 1. Overview of K-bearing materials with current or potential application in global agriculture.

K-bearing ore	K source	K_2O grade (wt%)[5,18,19]		Solubility (g L^{-1})[36–38]	Main advantages	Main disadvantages
		ore	processed			
Sylvinite	KCl	10-35	Up to 63.2	335.0 (25 °C)	Abundant resources High K_2O grade Medium processing cost Established supply chain	Localized distribution of reserves High transportation cost High chloride content (47.6 wt%) High salt index
n/a	K_2SO_4[A]	n/a	Up to 54.0	120.0 (25 °C)	Low-to-zero chloride content Sulphur content (18.4 wt%) Low salt index	High processing cost High transportation cost Partial agronomic know-how
Other evaporitic ores:						
Langbeinitite	$K_2Mg_2(SO_4)_3$	7-12	Up to 22.7	240 (20 °C)	Medium-to-high K_2O grade	Scarce resources and reserves
Polyhalite	$KMgCl_3{\cdot}6(H_2O)$	10-16	Up to 17.0	853 (25 °C)	Multi-nutrient carrier	High processing cost
	$K_2Ca_2Mg(SO_4)_4{\cdot}2H_2O$	n/a	Up to 15.6	27 (25 °C)	Low-to-zero chloride content	High transportation cost Limited agronomic know-how
Micas:						
Phlogopite	$KMg_3(Si_3Al)O_{10}(F,OH)_2$	3-7	n/a [B]	Time-dependent dissolution rate ~10^{-6}-10^{-9} mol m^{-2} s^{-1} (insoluble on agronomic timescale)	Abundant resources and reserves Worldwide distribution Low processing cost Low transportation cost Low-to-zero chloride content Multi-nutrient carrier	Low K_2O grade Low dissolution rate Limited agronomic know-how Contains Al
Muscovite	$KAl_3Si_3O_{10}(OH)_2$	3-7	n/a			
Biotite	$K(Mg,Fe^{++})_3AlSi_3O_{10}(OH,F)_2$	3-7	n/a			
Ultrapotassic syenite	$KAlSi_3O_8$	13-15	~16.9 [B]	Time-dependent dissolution rate ~10^{-10}-10^{-14} mol m^{-2} s^{-1} (insoluble on agronomic timescale)	Abundant resources and reserves Worldwide distribution Low processing cost Low transportation cost Low-to-zero chloride content Multi-nutrient carrier	Medium K_2O grade Very low dissolution rate Limited agronomic know-how Contains Al
Ultrapotassic syenite	Hydrothermal material (this study)	13-15	11.7	*Vide infra*	Abundant resources and reserves Worldwide distribution Medium processing cost Low transportation cost Low-to-zero chloride content Multi-nutrient carrier	Medium K_2O grade Limited characterization No agronomic know-how Contains Al

[A] The main production route for K_2SO_4 is not through mining of ores such as arcanite, which is extremely rare, but rather from chemical synthesis based on the reaction $2KCl + H_2SO_4 \rightarrow K_2SO_4 + 2HCl$ (Mannheim process). The process is operated at 600°C-700°C and incurs in high energy consumption and capital cost as well as equipment corrosion[19]. KNO_3 (K_2O up to 46.6; *S*=316 g L^{-1} (20 °C)), is obtained from chemical synthesis too. Several industrial processes are used in this case, including that one based on the double displacement reaction $NaNO_3 + KCl \rightarrow NaCl + KNO_3$. Overall global production is limited. Other soluble species such as KOH and K_2CO_3 are not discussed here.

[B] In micas, the main impurity is quartz. In ultrapotassic syenites the main impurities are mafic minerals, *i.e.* biotite, pyroxene, amphibole and Fe-oxides. Mafic minerals can be separated magnetically, and high purity K-feldspar can be obtained. The economics of the separation process is generally unfavorable.

2. EXPERIMENTAL

2.1 Reagents

The ultrapotassic syenite used in this study is the sample MCA41 described in detail elsewhere[18]. Briefly, the syenite was obtained from the Triunfo batholith, located in Pernambuco State, Brazil. The K-feldspar content was 94.5 wt%. The SiO_2, Al_2O_3 and K_2O content were 62.4 wt%, 17.0 wt% and 14.3 wt%, respectively. Hand-sized field samples were comminuted in a jaw crusher, and sieved to obtain particles with size <2 mm.

CaO (reagent grade, Alfa Aesar) was used as received. Due to storage, at the time of the experiments it was hydrated in $Ca(OH)_2$ (ESI 2).

The feed mixture for hydrothermal processing was obtained by jointly milling in dry conditions 21.28 g of ultrapotassic syenite (<2 mm) and 3.72 g of $Ca(OH)_2$, *i.e.* the hydrated form of the purchased CaO. The nominal Ca/Si molar ratio was 0.23, based on the assumption of both 100% $Ca(OH)_2$ and 0 wt% Ca in the ultrapotassic syenite. Milling was performed with stainless-steel balls loaded in a 50 mL alumina grinding jar pre-filled with Ar (Airgas, pre-purified grade 4.8) and subsequently evacuated. The mixture was ball milled (VQ-N high-energy vibrator ball mill, Across International) for 1 min. The milled powder (feed mixture) was subsequently transferred in a plastic container, and temporarily stored under Ar. Processing occurred within 20 min of milling operations.

Type II water (Ricca Chemical Company®, ACS reagent grade) was boiled and cooled down to room temperature in a stream of bubbling Ar. A stock amount was stored under Ar. Loading of the feed mixture into the hydrothermal vessel was handled under ambient conditions, therefore, air-contact with the feed mixture and water was unavoidable.

2.2 Hydrothermal processing

A schematic of the hydrothermal reactor used in this study (Parker, EZE-Seal®, 300 mL) is given in ESI 3. The reactor was loaded with 25 g of feed mixture and 100 mL of water. The reactor was sealed and the rotation of the impellor set at 400 rpm. The temperature set point of 200 °C was reached in approximately 40 min, and held for 5 h. The internal pressure of the reactor was ~14 atm. Subsequently, the reactor was cooled down with a water recirculating system, until the internal *T* reached ~60 °C (~15 min). The reactor was opened quickly, and the hydrothermal slurry transferred quantitatively in a glass beaker (*SA* ~44 cm^{-2}). The solid component settled at the bottom of the beaker, and the excess solution (supernatant) separated on top of it. The supernatant was dried on top of the solid phase overnight (18 h) in a laboratory oven set at 90±5 °C. An overall temperature profile for the process is given in ESI 4. The dried solid cake was homogeneously ground with an agate mortar and pestle to obtain a powder that we refer to as the *hydrothermal material* (ESI 5). A flow chart of the overall laboratory processing route is given in

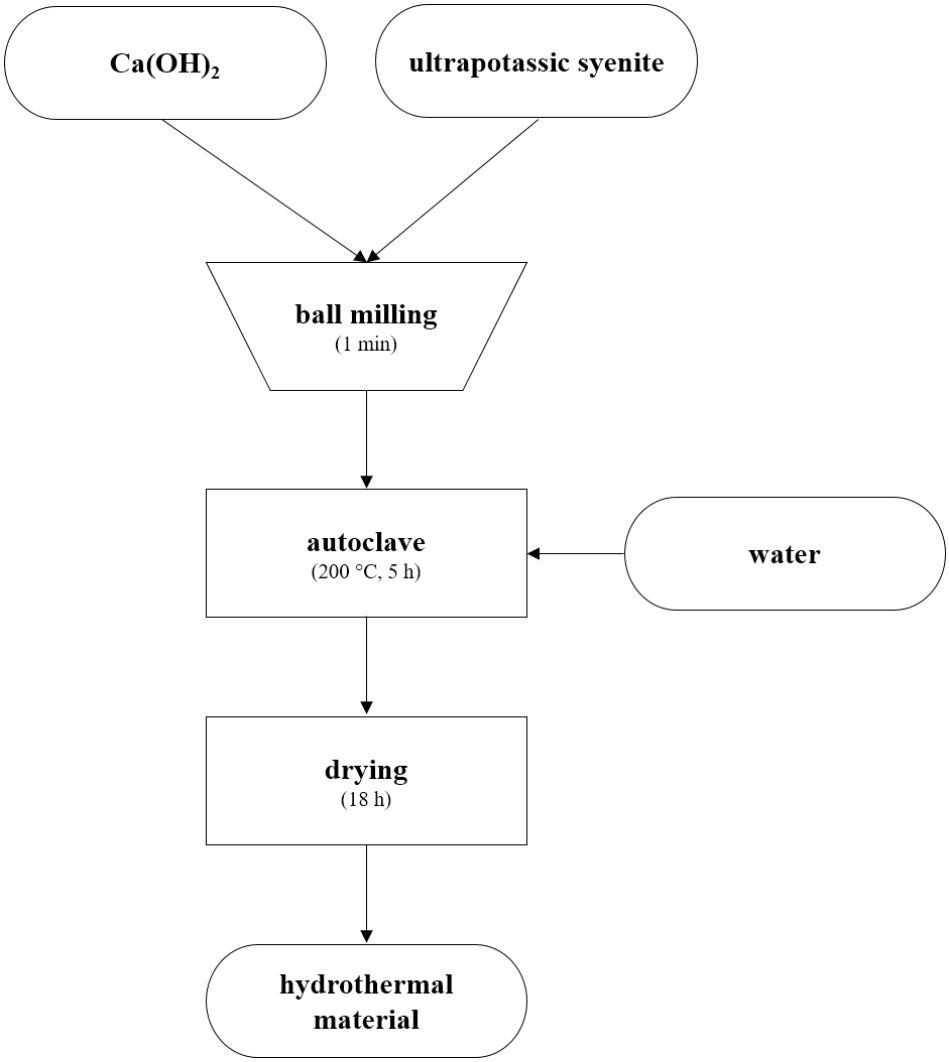

Figure 1 Flow chart of the laboratory processing route to synthesize the hydrothermal material. In this chart, the source of Ca is expressed as $Ca(OH)_2$ due to the high level of hydration of the CaO used in the experiment.

Figure 1. The mass of hydrothermal material was not measured. However, Loss of Ignition (LOI) experiments at 1000°C for 1 h (three replicates) showed a loss of 4.4±0.5 wt%, most likely due to water and/or carbonaceous content. Accordingly, the re-calculated mass of hydrothermal material was 26.1g. The long-term storage of the material occurred under Ar.

2.3 X-Ray Powder Diffraction (XRD)

The mineralogy of the hydrothermal material was determined by X-ray powder diffraction (XRD). The sample was micronized, loaded into a cup and put into a diffractometer (Panalytical X'Pert MPD) that used as X-ray source the $Cu_{K\alpha}$ radiation at 45 kV and 40 mA. Scans were run in the 2θ range 6°-90°, with a step size of 0.0131° and a counting time of 250 s $step^{-1}$. Once identified, mineral phases were quantified via Rietveld refinement. A few small peaks (1% of the overall diffraction patterns) could not be positively

identified and were ignored. An additional 1.1 wt% was attributed to panunzite, but this phase was not confirmed during observation of the material mounted in thin section. The amorphous content was determined quantitatively by adding and thoroughly mixing to the sample an equivalent weight fraction of Si powder (NIST SRM 640). A second XRD scan was run under the same conditions as the initial scan. A new Rietveld refinement was performed, permitting a comparison, adjusted for differences in scattering power, between the integrated intensity of the Si peaks and the integrated intensity of the known crystalline phases determined in the initial analysis. The difference between these values as a portion of the total was assumed to be due to the amorphous content of the sample. The final amount of each crystalline component is the result of the initial Rietveld refinement normalized to take into account the estimated amorphous content.

Samples showed a high degree of preferred orientation and overlapping peaks, requiring extensive manual fitting. Additionally, because of the preferred orientation and degree of overlap between microcline and orthoclase only one phase labeled "K-feldspar" is reported. Given several sources of uncertainties, XRD quantification can be considered only as an estimate.

2.4 Scanning Electron Microscope (SEM)

The hydrothermal material was mounted in thin sections (27mm×46mm, 30 μm thick, two-sided polish 0.5 μm diamond, borosilicate glass, acrylic resin; Spectrum Petrographics Inc.) and observed with a Scanning Electron Microscope (JEOL 6610 LV) operated in high vacuum mode ($<10^{-3}$ Pa). The accelerating voltage was 10-20 kV, the spot size 45-60, and the working distance 9-10 mm. Before observation, sections were carbon coated (Quorum, EMS 150T ES). In between studies, thin sections were stored under vacuum.

2.5 Electron Probe Micro-Analyzer (EPMA)

The chemical composition of the hydrothermal material mounted in thin section was determined with an Electron Probe Micro-Analyzer (EPMA) (JEOL JXA-8200), using an accelerating voltage of 15 kV, beam current of 10 nA and beam diameter of 1 μm. The mineral phases were analyzed with counting times of 20–40 s. From counting statistics, 1σ standard deviations on concentration values were 0.3-1.0% for major elements, and 1.0-5.0% for minor elements. Back-scattered electron (BSE) images and X-ray elemental maps (4.5cm×2.7cm) were obtained using a voltage of 15 kV, a beam current of 1 nA and a resolution of 10 μm. The use of such settings as well as operations in stage-rastered mode with a stationary beam avoided signal loss and defocusing of the X-ray. Due to possible damage to the mounting epoxy of the thin sections, EPMA analyses were carried out after SEM imaging. The thin section was mounted in a custom-made holder, which permitted access to and identification of individual particles to allow for analysis using multiple techniques.

2.6 Laser-diffraction Particle Size Distribution (PSD)

The Particle Size Distribution (PSD) of powder samples was determined with a laser-diffraction particle size analyzer (Beckman Coulter Inc., LS 13 320) equipped with a custom-made module for sample introduction. Samples were suspended in water during the analysis and were not sonicated.

2.7 Specific Surface Area according to Brunauer Emmet and Teller (BET-SSA)

Specific Surface Area according to Brunauer, Emmet and Teller (BET-SSA) was determined with a Micromeritics ASAP 2020 surface area and porosity analyzer[39]. The gas used for adsorption was N_2. Samples (~0.5 g) were degassed at 200 °C until a constant degassing rate of 10^{-5} mmHg min^{-1} was reached in the sample tube (12 h). SSA was determined on the adsorption branch of the isotherm with the multi-points method in the p/p_0 range 0.08-0.35. However, the complete adsorption (up to $p/p_0 = 0.99$) and desorption isotherms were recorded.

2.8 Leaching experiments and Inductively Coupled Plasma Mass Spectroscopy (ICP-MS)

Leaching experiments for both the ultrapotassic syenite and the hydrothermal material were run in batches, meaning that 0.3 g of solid material were contacted with 3 mL of leaching solution (m_S:m_L=0.1), and rotated continuously for 24 h in a closed 15-mL polypropylene test tube. Before starting the rotation, vials were pre-filled with Ar. Mass-transfer limitations are considered negligible under the given stirred conditions. To mimic an acidic soil solution, an aqueous solution of HNO_3 at initial pH=5 was used as the leaching solution. The stock leaching solution was prepared by appropriate dilution of standardized HNO_3 0.1M (Alfa Aesar) in boiled water, followed by vigorous Ar bubbling for ~15 min. At the end of the experiment the suspension was filtered (Whatman 13 mm GD/X, 0.45 µm), and diluted 1:100 in standardized HNO_3 0.1 M. Filtering occurred within 15 min of stopping the rotator. Each leaching experiment was performed in triplicates. Error bars represent the standard deviation of experimental data over the three replicates. Experiments were conducted at room temperature (20±3°C). The temperature of the leaching solution remained constant upon contact with the hydrothermal material.

Inductively Coupled Plasma Mass Spectroscopy (ICP-MS) was used to determine the concentration of K, Al, Si, Na, Ca, and Mg in the diluted leachate (ICP MS, Agilent Technologies 7700 Series). The instrument is equipped with an Octopole Reaction System (ORS) that was run in "He mode" (He=4.0 mL min^{-1}) except for Ca, which was determined in "no-gas mode". A solution at 1 ppm of In (Sigma-Aldrich, TraceCERT®) was used as the internal standard.

Leaching tests are not devoid of intrinsic limitations. Particularly: i) the pH and other properties such as ionic strength and conductivity of the leaching solution change over the 24 h experiment. Furthermore, the actual pH of leaching was higher than the initial nominal pH (ESI 6). Here, we intentionally choose to operate in non-buffered conditions, to avoid introducing in the system additional chemicals such as an

acetic buffer, which would complicate both the dissolution rate and the overall experimental protocol ii) the leaching system is batch, meaning that the solution is progressively enriched with several ions, leading to common-ion effects and possibly re-precipitation in the leaching vial of silicate phases iii) although ground in mortar, the hydrothermal material may present heterogeneities that made it difficult to obtain a truly randomized sampling iv) PSD and SSA of each of the composing mineral phases change over time due to continue dissolution, and cannot be determined. Leaching results are given in ppm of available element in the hydrothermal material ($mg_{element}/kg_{material}$), and are not normalized to consider such variations in PSD and SSA and v) no speciation analysis was performed, either theoretical or experimental; the elemental concentration is the total atomic concentration as detected by ICP-MS.

3. RESULTS and DISCUSSION

3.1 Mineralogy

X-ray powder diffraction (XRD) was used to determine the mineralogy of the hydrothermal material (Figure 2). The diffraction pattern is given in ESI 7. XRD analysis detected K-feldspar ($KAlSi_3O_8$) and new mineral phases formed during hydrothermal processing and/or drying, namely hydrogrossular ($Ca_3Al_2(SiO_4)_{3-x}(OH)_{4x}$), α-dicalcium silicate hydrate ($Ca_2SiO_3(OH)_2$), 11 Å tobermorite ($Ca_5Si_6O_{16}(OH)_2 \cdot 4H_2O$) and amorphous material(s). Some of the mineral phases have been observed previously in literature studies on CaO-Al_2O_3-SiO_2-H_2O hydrothermal systems (Table ESI 1).

K-feldspar is the main mineral component of the ultrapotassic syenite used in the feed mixture[18]. In the hydrothermal material, the remaining K-feldspar detected by XRD accounted for 66.5 wt%, indicating a full conversion of 17.4 wt% of the original mineral, with the remaining existing as an altered phase. Hydrogrossular was 6.5 wt%, and based on molecular formula is the only calcium aluminum silicate hydrate. It was determined as plazolite (x=1.47) in the Rietveld refinement (ESI 7), but most likely it was a solid solution of phases with variable levels of hydroxyl ions replacement ($0<x<3$) as shown later with EPMA analysis. α-Dicalcium silicate hydrate and 11 Å tobermorite are 3.3 wt% and 3.2 wt%, respectively, and based on molecular formula are calcium silicate hydrate phases. Lastly, an amorphous component corresponding to 18.2 wt% was also detected in the hydrothermal material. Further to such main components, 1.2 wt% of albite and 1.1 wt% of panunzite were also detected by XRD.

Preliminary SEM observations of the hydrothermal material were made on the powder as such (ESI 8). Subsequently, it was mounted in thin section, for detailed exploration of morphological features (SEM) and chemical analysis (EPMA). Results (Figure 3, Figure 4, Table 2, ESI-EPMA) confirm XRD findings, although a high degree of heterogeneity was evidenced.

In the thin section, K-feldspar crystals could be distinguished (Figure 3a-b, Figure 4) and showed clear alterations with respect to the rock powder. Such alterations were evidenced by heterogeneous formations (Figure 3a-d) and EPMA chemical analysis (Figure 4, Table 2, ESI-EPMA). Chemical composition changed across feldspar size classes (d<50 μm; 50 μm<d<100 μm; d>100 μm), with the smaller crystals being richer in Ca and poorer in K, Si and Al (Table 2, ESI-EPMA). Note that solid-state mechano-activation could replace Ca with both surface and framework K at the milling stage, and such possibility could not be ruled out completely, especially for the smallest grains (ESI 9; ESI-EPMA). However, in the hydrothermal material, a distinct characteristic was that certain medium sized K-feldspar grains (50 μm<d<100 μm) were unusually enriched in Ca (ESI 9; ESI-EPMA), which was not the case for crystals with equivalent size in the feed mixture. This was an evidence of insertion of Ca atoms in the feldspar framework during hydrothermal processing. Note that such conclusions are not immediately evident from

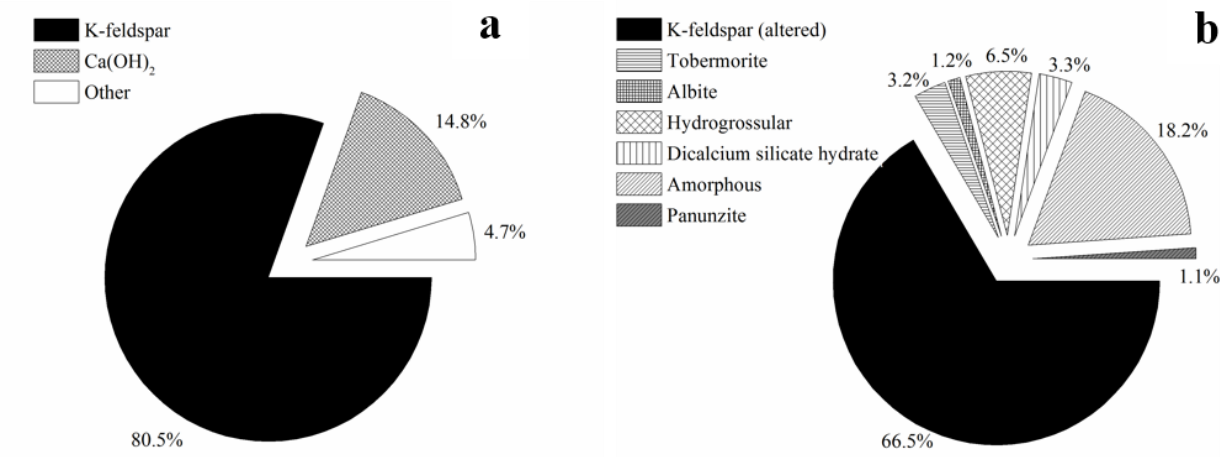

Figure 2 Mineralogical composition of (a) feed mixture and (b) hydrothermal material. All numbers are wt%. The mineralogical content of the feed mixture is calculated from data reported for ultrapotassic syenite MCA41 by Ciceri *et al.*[18] assuming 100 wt% $Ca(OH)_2$ as the Ca source; *other* is the fraction of varietal and accessory composition, which may contain Ca as well[18]. In the hydrothermal material, panunzite is a phase that was not confirmed independently. Water content (not shown) can be presumed to be 4.4 wt% as determined by LOI experiments. Accordingly, K_2O in the hydrothermal material was re-calculated to be 11.7 wt%.

median concentration values (Table 2), highlighting a high degree of compositional heterogeneity. K-feldspar crystals were often surrounded by hydrogrossular, α-dicalcium silicate hydrate and 11 Å tobermorite (Figure 3a-d). Cracking and fracturing were additional common features of K-feldspar (Figure 3a-b).

Hydrogrossular crystals had a predominantly spherical shape ~1 μm in diameter, although some crystals were ~5 μm in diameter (Figure 3g). Hydrogrossular was found either surrounding K-feldspar or scattered across the material. More rarely, it occurred as larger aggregates of up to ~30 μm and with a colloidal appearance (Figure 3h; ESI 9). It was difficult to distinguish 11 Å tobermorite from α-dicalcium silicate hydrate based only on morphology and textural characteristics. Tobermorite occured in two main forms: i) as numerous individual crystals, more developed, up to 20 μm long and 1 μm wide (Figure 3b) or ii) as an aggregate within clump-like formations and clusters, with each composing crystal again <1 μm (Figure 3c-f). In both occurrences, tobermorite had a fibrous texture, appearing commonly as fine needles. The texture of α-dicalcium silicate hydrate was similar to the first type of tobermorite occurrence, but it was more developed and well-formed (Figure 3d). Additionally, a distinction between the two minerals was that for tobermorite some point analyses showed a K enrichment as high as 5.3 wt%, and for α-dicalcium silicate hydrate the total oxide content tended to be lower (ESI-EPMA).

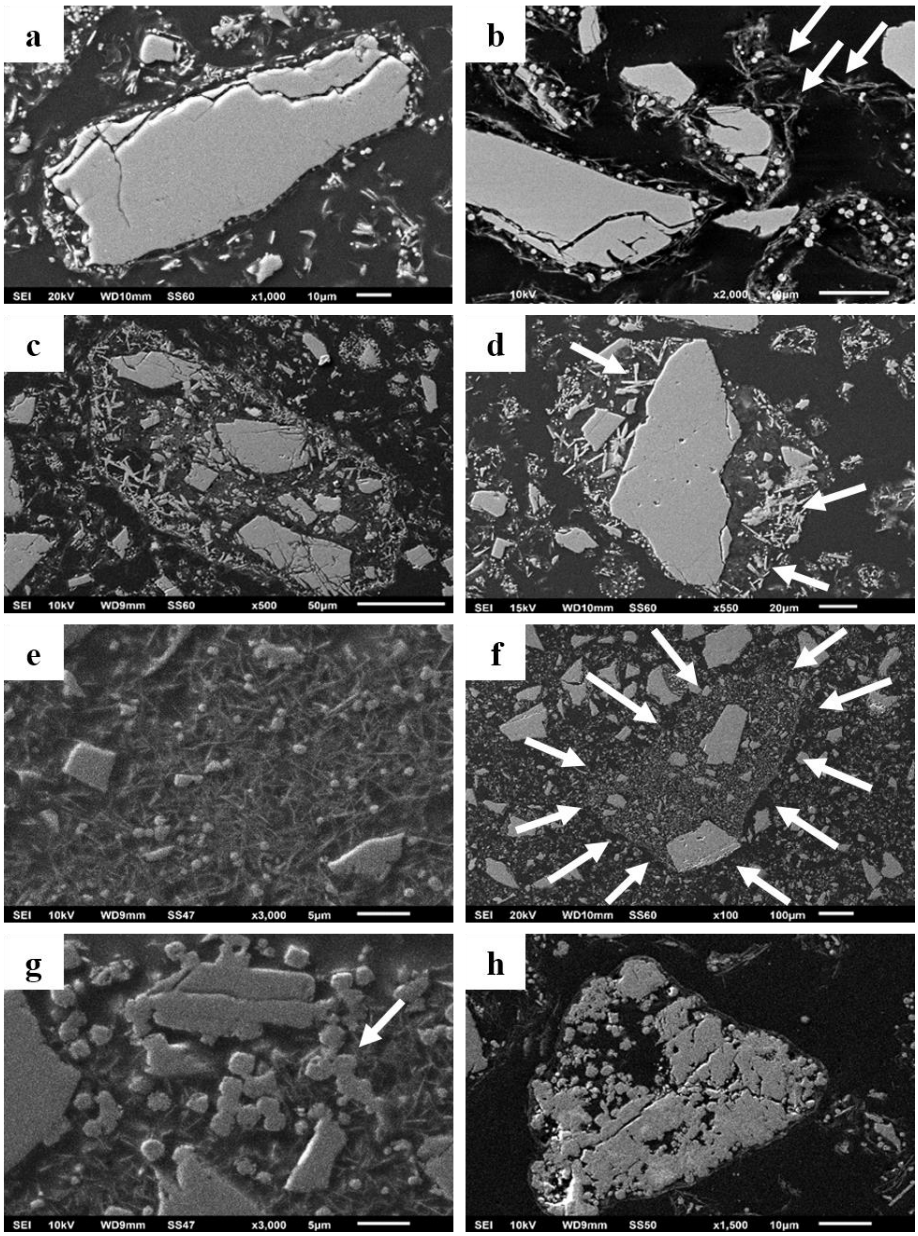

Figure 3 SEM micrographs of the hydrothermal material mounted in thin section. (a) and (b) show particles of altered K-feldspar with evident internal cracking, and rim of fine Ca minerals possibly nucleating at the edge of the grain (compare Figure 4a); small round particles (hydrogrossular) and elongated crystals (α-dicalcium silicate hydrate and tobermorite) are visible. Arrows in (b) point at elongated particles of tobermorite located outside the rim of calcium minerals; (c) and (d) show extremely heterogeneous clump-like formations. The clump is delimitated by a rim of small particles of Ca minerals that encapsulates altered K-feldspar, α-dicalcium silicate hydrate and tobermorite (compare Figure 4b). A whitish background haze is observed within the clump which may be attributed to fine tobermorite crystals. In (d), arrows point at thick elongated crystals of α-dicalcium silicate hydrate. Such crystals are distinguishable from those of tobermorites shown in (b), which appear much thinner. (e) High-magnification detail of elongated and fibrous tobermorite crystals; some round particles of hydrogrossular are also visible (f) cluster. Arrow point at the edge of the cluster to highlight its overall size and shape (g) high magnification detail of round hydrogrossular crystals. The arrow points at an area where multiple crystals seem to intergrow together (h) Extreme case of relatively large mass of intergrown hydrogrossular. Note that the particles diameters observed here match the results from laser-diffraction PSD reported in Figure 6. Images of K-feldspar powders before hydrothermal processing are given in Ciceri *et al.*[18].

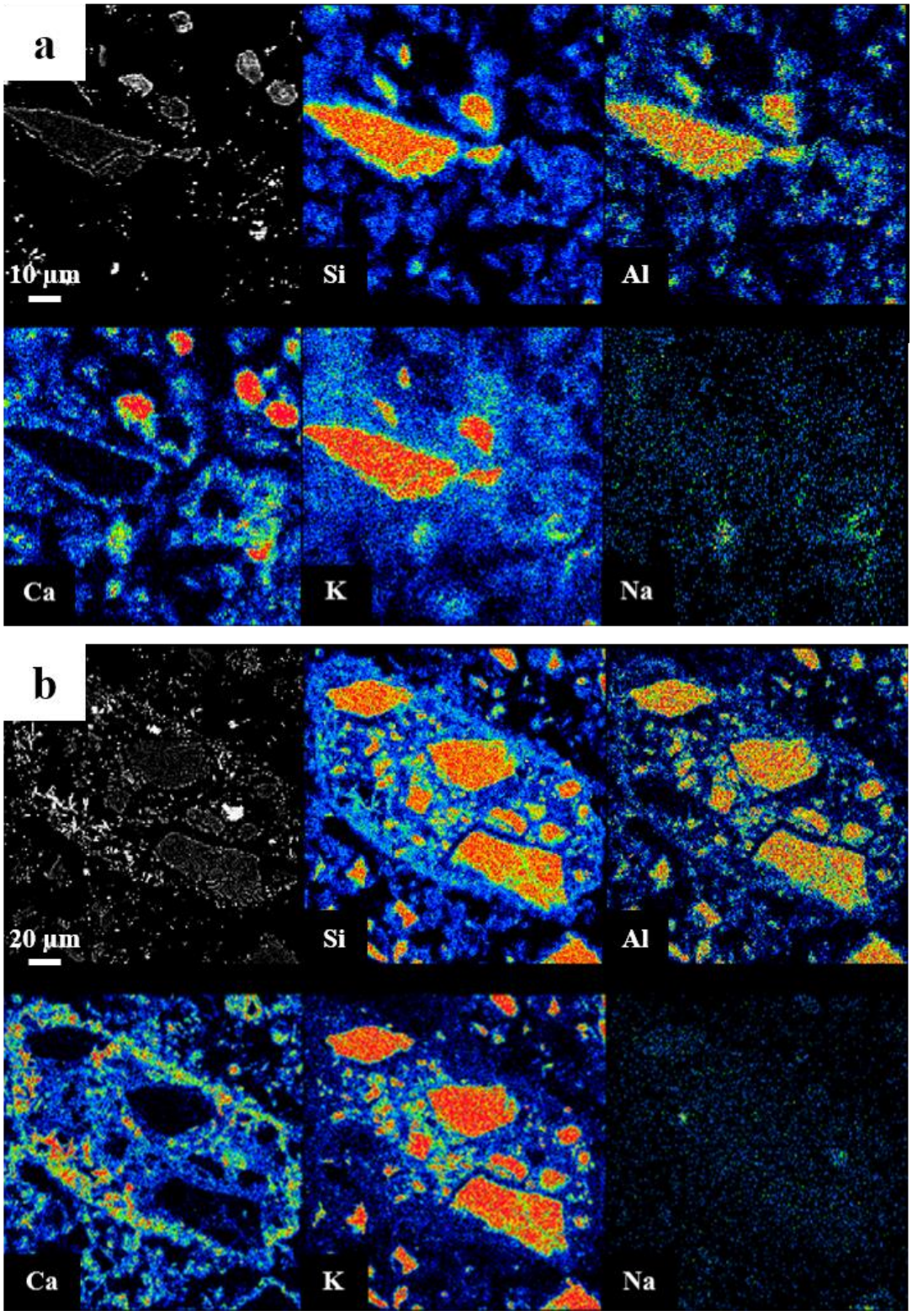

Figure 4 Electron Probe Micro-Analyzer (EPMA) X-ray elemental maps of (a) altered K-feldspar and (b) clump-like formations. Color scales are omitted for clarity. Hotter colors correspond to higher concentrations of an element; colder colors correspond to lower concentrations. Color-scale intensities are comparable for the same element, but not across elements. Particles reported here are the same as Figure 3(b) and Figure 3 (c). Additional maps are reported in ESI 9. Scale bar in the top left inset applies to all subsequent images.

Table 2 Median oxide and elemental (F and Cl) concentration per mineral phase in the hydrothermal material. All numbers are wt%. Data are obtained by EPMA analysis on a large number of observations (ESI-EPMA). Balance to 100 wt% is likely due to water content.

Mineral phase	K_2O	Al_2O_3	SiO_2	Na_2O	CaO	MgO	P_2O_5	TiO_2	MnO	FeO	SO_3	F	Cl	Total
Altered K-feldspar (<50µm)	13.4	17.1	59.8	0.5	0.3	0.0	0.0	0.1	0.0	0.4	0.0	0.0	0.1	92.8
Altered K-feldspar (50µm<x<100µm)	14.6	18.4	64.3	0.6	0.1	0.0	0.0	0.1	0.0	0.4	0.0	0.0	0.0	98.5
Altered K-feldspar (>100µm)	15.0	18.3	64.1	0.6	0.1	0.0	0.0	0.1	0.0	0.5	0.0	0.0	0.0	98.6
Hydrogrossular	0.6	13.4	17.2	0.0	27.4	0.3	0.0	0.0	0.0	0.6	0.1	0.2	0.6	66.1
α-Dicalcium silicate hydrate	1.1	1.0	12.8	0.2	20.0	0.1	0.0	0.0	0.0	0.1	0.0	0.0	0.7	40.5
11 Å Tobermorite	1.2	2.9	16.4	0.2	17.1	0.1	0.0	0.0	0.0	0.3	0.0	0.0	0.7	41.2
Amorphous	6.7	9.9	30.2	0.3	6.1	0.0	0.0	0.0	0.0	0.2	0.0	0.1	0.8	59.9

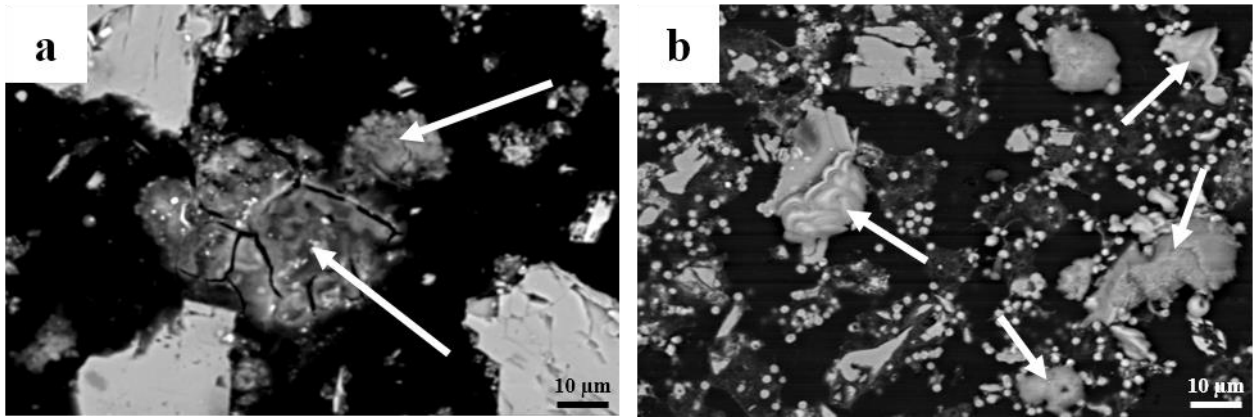

Figure 5 Electron backscattering images obtained with the Electron Probe Micro-Analyzer of (a) an amorphous compound and (b) carbonaceous species.

An additional morphological feature of the hydrothermal material was the appearance of large structures on the order of ~2 mm, which we refer to as *clusters* (Figure 3f). They were often round, and richer in Ca- and K- substituted alumino silicate hydrates than the rest of the hydrothermal material. Occasionally, they exhibited outer rims enriched in α-dicalcium silicate hydrate and tobermorite. It is likely that such formations are due to the binding nature of calcium silicate hydrates[40]. Indeed, C_2S phases are often observed as agglomerated phenocryst in concrete[41]. A rigorous quantitation of the density of the hydrothermal material was not performed. However, visual observations of the clusters (Figure 3f) show a large fraction of empty space, and suggest low density for such formations. This may explain, at least partially, the macroscopic appearance of the hydrothermal material when compared with that of the rock powders (ESI 5).

Lastly, various mineral phases could contribute to what is detected as amorphous by XRD such as i) severely altered K-feldspar ii) crystalline, but very small particles iii) truly amorphous compounds, for example poorly crystallized non-stoichiometric calcium-silicate-hydrate (C-S-H). However, exploration of the sample with EPMA showed that the amorphous phase occurred in two main forms: i) as material generated from the original K-feldspar, from which it maintains a similar weight proportions of K, Al and Si, but that has been so severely altered that the total oxides content is very low; such a material presents expressive Ca content ii) as completely anhedral forms (Figure 5a), with no evidence of crystallinity or stoichiometric proportions of oxides attributable to known silicates, oxides, chlorides, carbonates or sulfides (ESI-EPMA). A detailed observation of thin sections revealed also the presence in the hydrothermal material of carbonaceous phases that are not detected by XRD (Figure 5b) and that are not attributable to impurities in the CaO reagent (ESI 2). This is likely due to concentrations below the detection limit. Such carbonates occurred subordinately and were mainly non-stoichiometric K-Ca-carbonates (atomic ratio Ca/K between 7 and 28; ESI-EPMA), in crystalline aggregates approximately 5-10 μm in diameter (Figure 5b). The crystals presented two main habits, tabular or prismatic. Carbonates were confirmed independently by an acid-base titration as well as a qualitative carbonate spot test (ESI 10; ESI 11).

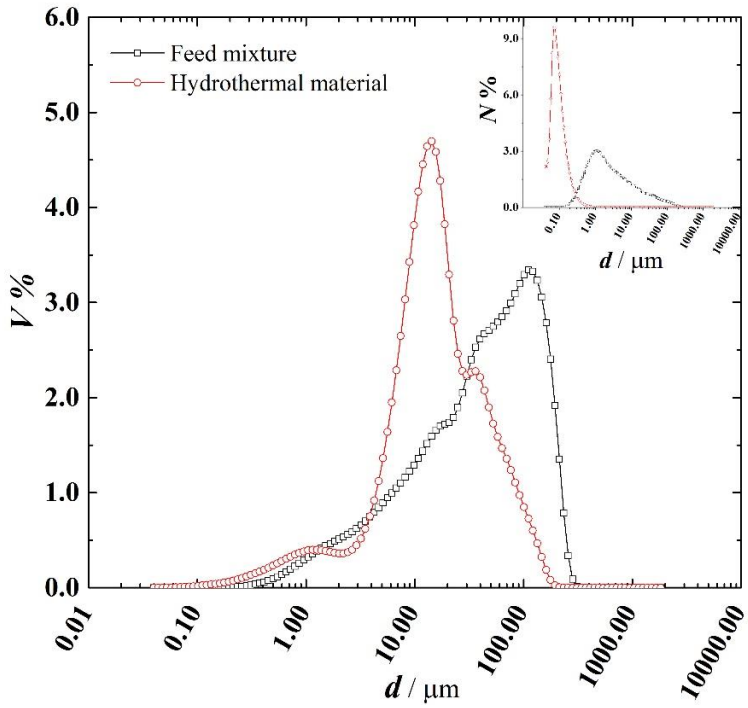

Figure 6 Particle Size Distribution (PSD) based on both volume percentage *V*% (main figure) and number of particles percentage *N*% (inset). Curves for both the feed mixture ($Ca(OH)_2$ + ultrapotassic syenite) and the hydrothermal material are shown. Specific Surface Area according to the BET method (BET-SSA) is 15.1 m^2 g^{-1} for the hydrothermal material and 46.9 m^2 g^{-1} for the feed mixture (rock powder+CaO).

3.2 PSD and BET-SSA

The Particle Size Distribution (PSD) of the feed mixture ($Ca(OH)_2$ + ultrapotassic syenite) is compared with that of the hydrothermal material in Figure 6. It is shown that after processing particles are smaller. Based on volume, three main populations are observed at ~30 μm, ~10 μm and ~1 μm, respectively. Therefore, processing shifts the major population peak of one order of magnitude, from ~100 μm in the feed mixture to ~10 μm in the hydrothermal material. The same shift is observed based on number of particles, from ~1 μm in the feed mixture to ~0.1 μm in the hydrothermal material. These observations are consistent with the size of the particles observed with the SEM (Figure 3). Overall, PSD can be used as a quick, efficient and inexpensive way to assess the efficiency of the process since the main size population in the rock powder and in the hydrothermal material shrink and grow, respectively, with the progressive conversion of K-feldspar.

The Specific Surface Area according to the BET method (BET-SSA) was 15.1 m^2 g^{-1} for the hydrothermal material and can be reasonably considered ~1 m^2 g^{-1} for the rock fraction in the feed mixture[18]. A comparison between surface areas of the hydrothermal material and the rock fraction is then consistent with a population of smaller particles in the processed material. The N_2 adsorption isotherm of the hydrothermal material (Type III according to BET classification) does not show any appreciable hysteresis (ESI 12).

3.3 Elemental leaching

Results from leaching tests for both the ultrapotassic syenite and the hydrothermal material are reported in Figure 7. Since actual pH conditions, PSD and BET-SSA are different for the two solid materials, results are compared only for a qualitative visualization of the order of magnitude of the elemental availability. In the hydrothermal material, there are 14,065±744 ppm_K available for dissolution, which is equivalent to 14.5% of the total K content of the feed mixture. Therefore, at 24 h potassium is two orders of magnitude more available than in the original ultrapotassic syenite leached at the same initial pH. For Si, Al and Ca availability is 1,520±132 ppm_{Si}, 222±38 ppm_{Al}, and 335±20 ppm_{Ca}, respectively, corresponding to 0.6%, 0.3% and 0.2% of the total content of Si, Al and Ca, in the feed mixture, respectively. The Ca in the varietal composition of the ultrapotassic syenite is taken into account in this calculation[18]. Na and Mg were also monitored because they are a major component of varietal composition and important elements for soil scientists[18]. Na can lead to potential soil salinization and Mg is a plant micronutrient. In the hydrothermal material there are 6.5±0.3 ppm_{Na} and 6±1 ppm_{Mg} available for dissolution, equivalent to 0.2% of both the total Na and Mg content in the feed mixture. The overall availability of Na is low and decreased in the hydrothermal material with respect to the ultrapotassic syenite.

Leaching tests provide information on the chemical stability of the mineral phases upon contact with water. Here, chemical stability must be understood in relation to the ability to release plant nutrients, and need to be contextualized in the agronomic context. As an example, the fraction of available Si and Ca nutrients in the hydrothermal material was in absolute very little, 0.6% and 0.2%, respectively. Although dissolution-reprecipitation may occur, this is evidence of the general chemical stability of all the calcium silicate phases under the given leaching conditions. Nevertheless, the absolute amount of nutrients available may be significant for plants. For reference, in the soil solution Si concentrations are in the order of 0.09-23.4 $mg_{Si}\ L^{-1}$, to be compared with the value of 152 $mg_{Si}\ L^{-1}$ in the leaching solution reported herein[42]. Note also that the actual leaching solution was diluted in concentrated HNO_3 before ICP-MS analysis, and this may cause a precipitation of Si species in the diluted vial[43].

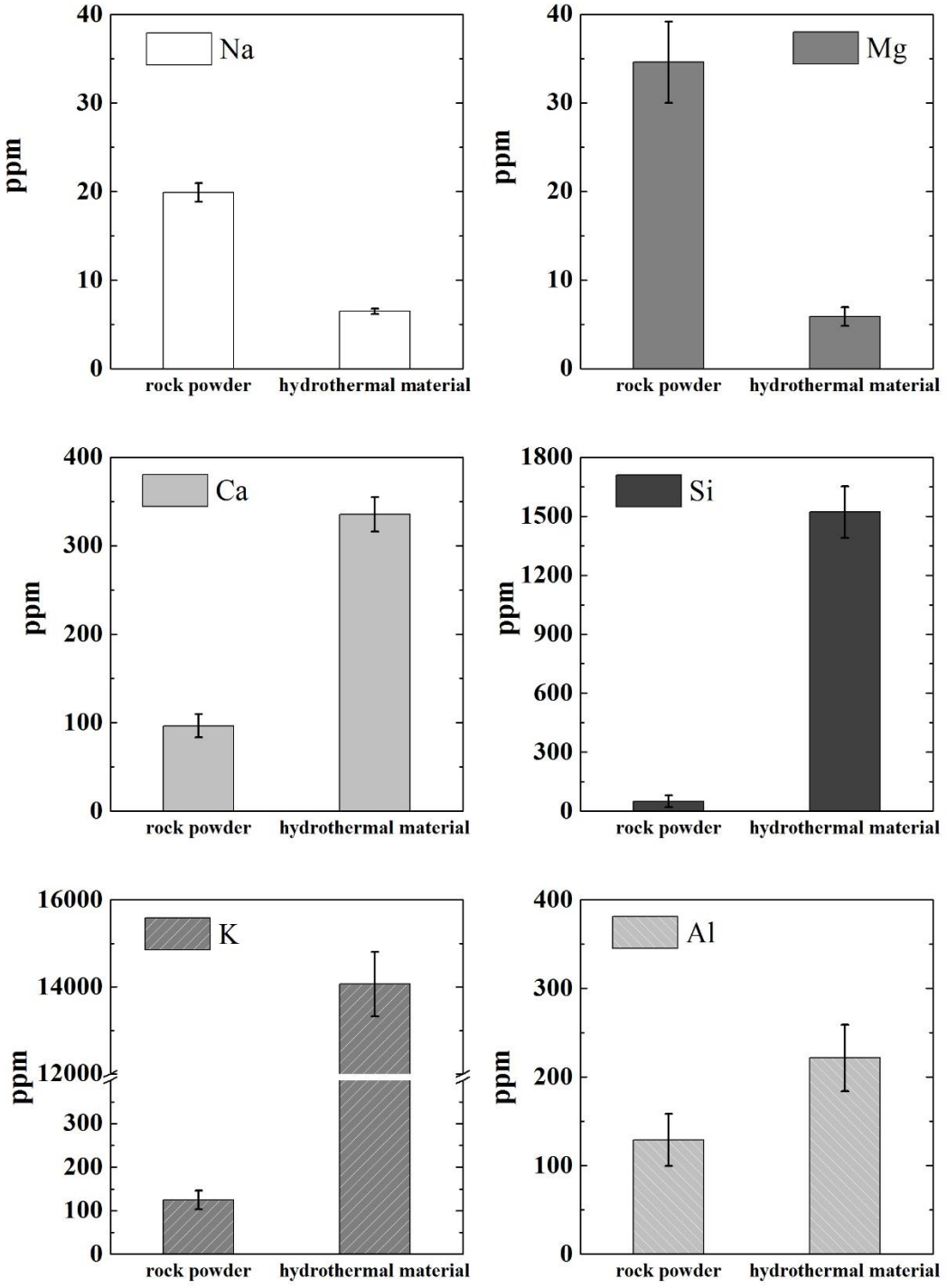

Figure 7 Elemental release from the rock powder (ultrapotassic syenite) and hydrothermal material. Leaching conditions: batch test under rotation, 24h, m_S:m_L=1:10. HNO_3 at nominal initial pH=5 as the leaching solution. All values (ppm), refer to the mg of element analyzed in solution by ICP-MS per kg of solid material. Note that the initial BET-SSA and PSD were different for the two materials: rock powder (initial pH=5, BET-SSA=17.3 m^2 g^{-1}, powder obtained from ball milling 1 min the fraction <2 mm described in the Reagents section); hydrothermal material (initial pH=5, BET-SSA=15.1 m^2 g^{-1}, PSD reported in Figure 6).

3.4 Hydrothermal chemistry considerations

The major potassium alumino-silicate (KAS) detected by XRD in the hydrothermal material was K-feldspar ($KAlSi_3O_8$). Calculations based on XRD data (Figure 2) showed that 14.0 g of K-feldspar were fully converted during processing. PSD analysis confirmed that the size population attributable to K-feldspar was reduced in the hydrothermal material with respect to the feed mixture (Figure 6). However, K-feldspar remains the main component of the hydrothermal material (66.5 wt%), and therefore also the main K-bearing phase. This is a carefully engineered feature of the material. A complete transformation of K-feldspar would be cost prohibitive, and would generate an excessively large amount of soluble K in the soil solution. However, note that what is detected by XRD as K-feldspar, is in fact an altered mineral phase. *Structural* alteration was evidenced by the imaging study (Figure 3a-d). Furthermore, the N_2 adsorption isotherm lacked hysteresis (ESI 12), which can be explained considering that cracks, fractures or other porous structures do not generate a hysteretic behavior if they are in the order of micrometers (Figure 3(a-b)), although their contribution to surface area is still captured by the BET-SSA value. Strain-induced fracturing and distortions in the unit cell of K-feldspar due to Ca insertion are a probable cause of the cracking effect mentioned above[44]. *Chemical* alteration was evidenced by elemental maps (Figure 4), point concentrations (Table 2, ESI-EPMA), as well as detailed exploration of the sample (ESI 8, ESI 9). Indeed, a feature of the hydrothermal material is that the smallest grains of altered K-feldspar particles showed a non-stoichiometric elemental content, highly deficient in K and enriched in Ca (Figure 4, ESI 9, ESI-EPMA). Regardless the size, no single grain of K-feldspar preserved its original composition, and calcium minerals were observed at the interface between K-feldspar grains and the hydrothermal solution. It was not clear if such phases originated from the insertion of Ca in the feldspar or rather re-precipitated from the solution due to local saturation. Here, the mechanism of alteration is not discussed in detail, although we point out that in absence of an alkaline environment, much higher temperatures (600 °C) would be required to observe a significant exchange between K in the feldspar and alkali ions from the hydrothermal solution[45]; in alkaline environment from NaOH or KOH K-feldspar did not show appreciable alteration[24], unless the temperature was at least 240 °C, leading to kalsilite[46]. The data presented in this work may therefore be the result of a concurrent hydrolytic framework dissolution mediated by OH^- ions and an exchange of K ions for Ca ions. Overall, the contribution from altered K-feldspar to the leaching-available K cannot be easily resolved, unless a mechanical separation of such a phase is carried out. Assuming for both altered and unaltered K-feldspar the same dissolution rate, and an actual pH of leaching of 12 units (ESI 6), then the amount of leaching-available K would be in the order of 13-189 ppm_K (ESI 6), which is negligible when compared with the data reported in Figure 7. This confirms that altered K-feldspar acts as a major nutrient reservoir for potential slow release over the long term, but is not likely to be responsible for K short-term release probed in the leaching experiment. Mass

balance calculations (ESI 11) show that the fraction of K in the K-feldspar that was completely converted during processing could provide all the K available in the leaching test. Such a K is likely to be located in K-substituted phases other than altered K-feldspar, or in the soluble K-carbonate fraction not detected by XRD, but evidenced by EPMA analysis (Figure 5, ESI-EPMA). Possibly, the hydrothermal material contains at least three K-releasing components: a fast-release component from carbonates, a medium-release component from K-substituted phases and a slow release component from altered K-feldspar.

The major calcium aluminum-silicate hydrate (CASH) phase detected by XRD in the hydrothermal material was hydrogrossular ($Ca_3Al_2(SiO_4)_{3-x}(OH)_{4x}$; $C_3A_2S_{3-x}H_x$). Within the broader hydrogarnet group, hydrogrossular defines a class of minerals where the incorporation of $4OH^-$ in place of a SiO_4^{4-} tetrahedron occurs, generating grossular (x=0), hibschite (x=0.2-1.5), katoite (x=1.5-3) and their solid solutions. In artificial systems, hydrogrossular is observed in concrete as the only calcium aluminum silicate hydrate, and is often detected as small crystals (1.5–4 μm) in the hydration product of autoclaved materials[32,47]. Increasing Si content in hydrogrossular influences the morphology of its particles with grossular appearing as octahedral-to-round crystals, hibschite as round crystals and katoite as cuboid crystals[24,48] (Table ESI 1). A comparison of micrographs of the hydrothermal material (Figure 3) with PSD data (Figure 6) reveals that in our experiments the hydrogrossular phase was mainly in the form of round particles in the order of ~1 μm (Figure 3g), suggesting hibschite rather than katoite. EPMA analysis showed a content of ~30 wt% of SiO_2, in agreement with expected composition for hibschite (Table 2; ESI-EPMA). Note that the SiO_2 content is also in relatively good agreement with the theoretical value of 22 wt% in the plazolite phase used in the Rietveld refinement. Together with K-feldspar, hydrogrossular is the key Al-bearing mineral. In the leaching test, the availability of Al from the hydrothermal material increased with respect to that of ultrapotassic syenite, although it remained comparable. However, the actual leaching pH of the rock powder is ~6 and that of the hydrothermal material is ~12 (ESI 6). The higher the pH the higher the solubility of Al, suggesting that in soils buffered at acidic pH, Al should be almost completely unavailable from the hydrothermal material. The level of K incorporation in the hydrogrossular crystals was little (Table 2).

The calcium silicate hydrates (CSH) were α-dicalcium silicate hydrate (α-$Ca_2(SiO_3OH)(OH)$; α-C_2SH), and 11 Å tobermorite ($Ca_5Si_6O_{16}(OH)_2{\cdot}4H_2O$; $C_5Si_6H_5$). Hydrothermal synthesis of α-dicalcium silicate hydrate has been reported previously[40,49,50]. The Ca/Si molar ratio in solution governs the formation of crystalline α-C_2SH (Ca/Si=2) with respect to that of other poorly crystalline and non-stoichiometric calcium-silicate-hydrate (Ca/Si<1.75)[50]. Therefore, α-C_2SH is likely to form in calcium-rich environments, at incipient reaction, whereas tobermorite would form later, as a phase evolving from metastable calcium-silicate-hydrates[51,52]. Tobermorite has been observed for initial bulk molar

composition at Ca/Si=0.8-1.0 and processing times in the order of days[53–55]. Al accelerates the transformation of calcium-silicate-hydrates into tobermorite[51,53-56]. The incorporation of Al^{3+} in place of Si^{4+} requires introduction of interlayer ions to maintain charge neutrality, generally Na^{+}, K^{+} or Ca^{2+}, yielding tobermorites with high CEC of ~0.7 meq g^{-1} [50,54,57,58]. Several crystal shapes have been reported for tobermorites, including platy, lath-like and fibrous crystals[24,55]. This latter type was confirmed in this study (Figure 3b, Figure 3e). K-substituted tobermorites (kalitobermorite) are extremely rare in nature[59]. However, in the hydrothermal material, tobermorite was shown to contain both K and Al (Table 2, ESI-EPMA). Overall, the absolute amount of potassium in tobermorite was little, and in the leaching experiment it was likely masked by the immediately available K component. Lastly, in the hydrothermal material an additional C-A-S-H phase was observed, likely a poor-to-no crystallinity compound detected as amorphous by XRD. Such an amorphous was shown to have an extremely variable composition (ESI-EPMA), and to contain K and Al further to Si and Ca. It is not clear what its elemental leaching may be.

Further to XRD phases it has been demonstrated that the hydrothermal material contains carbonaceous species too (Figure 5b, ESI-EPMA), which contribute to regulate the pH of aqueous solutions that contact the material, and can be used to capture atmospheric CO_2. Carbonation is not attributable to the feed mixture, which contains 0.8 wt% of $CaCO_3$ in the $Ca(OH)_2$ reagent (0.12 wt% in the feed mixture; ESI 2) or from atmospheric CO_2 in the hydrothermal reactor[†]. Solid-state carbonation of mineral phases during production and mounting of the powder in thin section should be negligible. Carbonation is likely to arise from the drying step. Liu *et al.*[24] reported a remarkable content of carbonates ($CaCO_3$+K_2CO_3+$K_2Ca(CO_3)_2$) between ~15 wt% and ~20 wt%, which was attributed to carbonation of the supernatant during the drying step. The amount of K_2CO_3 that would justify the leaching of Figure 7 is equivalent to 2.50 wt% of the hydrothermal material, which is an amount sufficiently low to be possibly undetected by XRD. However, as demonstrated in ESI-EPMA carbonates formed during processing are complex species with a variable atomic ratio K/Ca, and with solubility values not immediately available in the literature. Given the mineralogical complexity of the hydrothermal material, the leaching setup does not allow discriminating the origin of available K, but the data presented in this study suggest carbonaceous species as a likely responsible. Other potassium reservoirs such as altered K-feldspar, tobermorite or the amorphous phases are presumed to release K at a slower, and possibly more controllable rate than a water-soluble species such as carbonate.

[†] The volume of the hydrothermal reactor was 300 mL. At room temperature, the water and the feed mixture occupied 100 mL and 9.6 mL ($d_{\text{feed mix}}$ assumed to be 2.6 g mL^{-1}), respectively. When the reactor was loaded and sealed, air occupied a volume of 190.4 mL. Assuming i) air is dry, T=20 °C, P=101.325 kPa, d_{air}=1.2041 kg m^{-3} and ii) $[CO_2]_{air}$=400ppmv, then processing occurred in the presence of 91.7 µg of CO_2, equivalent to 0.0004 wt% of the feed mixture.

Leaching data (Figure 7) underscore the importance of linking nutrient availability to mineral phases, in order to forecast the agricultural performance of the material. Such data show that except for Na and Mg the elemental availability from the hydrothermal material is higher than in the ultrapotassic syenite leached at the same initial pH. For Ca, the availability is not immediately comparable because in the raw material it was available from varietal minerals whereas in the hydrothermal material it was artificially introduced by addition of $Ca(OH)_2$ to the system. A holistic overview of the hydrothermal material reveals that K-feldspar exhibited pozzolanic activity, which is a behavior unique to the $[K_2O\text{-}Al_2O_3\text{-}SiO_2]_{K\text{-}feldspar}$-$CaO\text{-}H_2O$ system[33,60]. Since such a system is far from thermodynamic equilibrium, it can be driven to intentionally redistribute framework elements into mineral phases that release beneficial nutrients to improve soil fertility.

3.5 Soil science considerations

A non-exhaustive list of desirable characteristics of a (tropical) fertilizer include: i) continuous potassium release to satisfy the needs of crops at different stage, and avoid both sudden saturation of the soil solution and excessive leaching ii) high residual effect to benefit plant nutrition over multiple agronomic cycles iii) ability to buffer soil pH at optimal levels for a given crop and microbiome iv) synergistic supply of micronutrients v) ability to support and improve soil mechanical strength and porosity vi) CEC improvement vii) low salt index viii) enhancement of Water Holding Capacity (WHC) and carbon storage capacity ix) affordability x) minimum hurdle for adoption by farmers xi) green-chemistry manufacturing process implementable at industrial scale, and that uses local resources. An overview of some properties of the hydrothermal material that fit that logic is provided below, suggesting its potential use as a multi-nutrient fertilizer for tropical soils.

Among physical properties, the hydrothermal material may be valuable to improve the soil pore space. In oxidic soil, both macropores (>75 µm; cannot hold water that is lost by gravity) and micropores (5-30 µm; hold water too strongly due to capillary forces) exist, but there are no intermediates mesopores (30-75 µm), which are those able to store water for long-term release[6]. Therefore, water holding capacity is low. The volume occupied by mineral particles is in a suitable range to improve mesopores population and reduce infiltration rates (Figure 6). This would also prevent dispersion of soil colloids and other fertilizers. Furthermore, it has been shown that solidified pastes of fine hydrogrossular and calcium silicate hydrates such as those composing the hydrothermal material have good flexural strength of 20mPa[52]. This characteristic could promote soil strength, without resulting in too large micro aggregate (>1mm) that would yield undesired infiltration rates. Although such reasoning needs experimental validation, it is clear that no K salt (KCl or K_2SO_4) can offer improvements to soil mechanics.

Among chemical properties, a prominent feature of the hydrothermal material is the availability of K (Figure 7). No robust protocol is available for determinations of the actual concentration of potassium in the soil solution at any given time of crop growth[7,13]. However, it is intuitive that due to high solubility (Table 1), KCl-fertilizers dissolve rapidly, resulting in a sudden increase of local K^+ and Cl^- concentrations, and drastically perturbing the equilibria between exchangeable and non-exchangeable K. Diffusion kinetics and pH-dependent ad-/ab- sorptions on small-sized clay minerals (negative charge) or oxides (positive charge) restrain and actively modulate an immediate saturation of the soil solution; however the major fraction of K is lost by deep-through leaching, a phenomenon exacerbated in tropical soils. We suspect that the hydrothermal material has an immediately soluble carbonaceous component, which would provide crops an immediate source of chlorine-free K. However, the unique opportunity presented here is offered by that small and yet critical portion of K that is redistributed among several phases, and from which it is likely to be available at a slower rate, not captured by the leaching experiment of Figure 7. Further to K, the hydrothermal material releases Si, Ca and Mg, and the high level of alkalinity (ESI 5) may partially substitute liming. Additionally, the mineralogy of the hydrothermal material suits tropical soils. Altered K-feldspar is a potential nutrient reservoir and contributes positively to soil mechanics, per principles discussed previously. Hydrogrossular stabilizes effectively Al, whereas α-dicalcium silicate hydrate, 11 Å tobermorite and amorphous calcium-silicate-hydrates are a source of Si, Ca, and alkalinity. Tobermorite acts as an ion exchanger especially if isomorphic incorporations such as those confirmed in this study occur (Table 2; ESI-EPMA). Furthermore, Al-substituted tobermorites show a higher selectivity for Cs, and possibly other heavy metals, which may be particularly useful to remediate contaminated soils[54,57,58]. The charge of such mineral phases is envisaged to further benefit soils. At lower pH, soil colloids are positively charged, holding anions such as nitrates and phosphates, whereas at higher pH negative charges hold the cations. The major mineral phases of the hydrothermal material are expected to have a negative surface charge, unless at extremely low pH. Feldspar itself has a negative surface charge above pH~2[61]. Although such value is influenced by the ionic strength of the soil solution, the altered feldspar fraction alone may aid limiting losses of immediately available K^+, contributing to an active sequestration of Al^{3+} and $Fe^{2+/3+}$ as well. Such benefits may be enhanced in the pore microenvironment[62].

Lastly, it is important to highlight some of the potential limitations of the hydrothermal material. Particles can be as small as hundreds of nanometers (Figure 6). This may cause health concerns, and may complicate blending and granulation with other nutrients. The long-term fate of Na, Al and other elements that are possibly carried by ultrapotassic syenites needs to be assessed, and so the compatibility with N and P fertilizers.

3.6 Green-chemistry considerations

In this section, we briefly discuss the broader green-chemistry and economic consequences of the hydrothermal process presented in this work. We do not aim to provide a complete life-cycle assessment, but rather an overview of the fit between green-chemistry principles and the synthesis of both KCl and the hydrothermal material (Table 3). For KCl, after mining and comminution two main routes exist for industrial production of fertilizers, namely electrostatic separation or thermal dissolution (95°C-115°C) followed by flotation. The selected processing route depends on grade and impurities of raw materials, as well as end-product specifications. Industrial flowsheets are simpler than other mineral processing plants (*e.g.*, Bayer process), but they are not obvious due to complex solubility equilibria in quaternary or quinary systems (*e.g.*, sylvinite-kieserite-carnallite-langbeinite-anhydrite)[19]. Although much has been done by the potash industry to meet sustainability goals, disposal of tailings and saline wastewater together with the use of alkylamine as frother agents do not allow to define the process as a truly green process.

The hydrothermal process presented in this work may suggest a valuable path forward to establish a role of green chemistry in fertilizer production. Necessary feedstocks are ultrapotassic syenite, CaO and water, which are abundant and affordable. Ultrapotassic syenites are available worldwide in bulk volumes constituting a virtually infinite resource of K_2O. Their mining occurs in conventional quarries for a low cost (~ US$ 10 ton^{-1}). CaO is obtained by roasting of limestone in rotary kilns, and is a raw material of several industries (*e.g.*, glass and cement), which operate based on already optimized costs and logistics. Dolomite ($CaMg(CO_3)_2$) may be a feasible alternative. Lastly, water quality, cost and availability vary regionally. We operated within a large excess of water, but general knowledge of concrete chemistry indicates that key properties of the hydrothermal material should not be compromised by minimization of processing water. Furthermore, seawater may be used in coastal areas, and may lead to the formation of KCl rather than carbonates. Further to raw materials, industrial scale up requires considerations on CAPEX and OPEX. The hydrothermal reactor (autoclave) is the major capital cost, whereas the operating cost is highly dependent on processing T and t as well as the design of the autoclave. Several industries make use of hydrothermal processing, and may inform the best strategy for an industrial implementation[34].

Lastly, from an environmental standpoint it is worth noting that the process does not produce any waste or byproduct. This is a key departure from processing technologies that aim to transform K-feldspar in soluble K salts[28-30]. The hydrothermal material is intended to be applied directly in soils, meaning that the altered K-feldspar fraction is not separated from the rest of the solid material. K-feldspar, hydrogrossular and tobermorite are naturally occurring mineral phases whereas α-dicalcium silicate hydrate and non-stoichiometric calcium-silicate-hydrates are components of concrete, and are not envisaged to pose major

environmental hazards. Furthermore, since only a portion of the initial K-feldspar is converted in new mineral phases, *T* and *t* are such to minimize the environmental footprint of the process. Finally, CO_2e emissions due to transport are reduced, since the hydrothermal material is manufactured locally and from local resources (ESI 1). CO_2e emissions due to processing are not explicitly addressed here, because of a high degree of uncertainty as a function of specific industrial equipment and geographical areas. An accurate quantitation of such emissions as well as those originating from sylvinite mining and processing will provide a true assessment of the environmental impact of both traditional and hydrothermal potash production.

Table 3 Fit of green-chemistry principles to both current KCl processing technologies (thermal dissolution/flotation) and the hydrothermal route proposed in this study. Category values (*yes*, *partial* and *no*) are a preliminary assessment and need further validation by the relevant scientific communities.

PRINCIPLE	FULLFILMENT OF THE PRINCIPLE	
	KCl	**Hydrothermal material**
PREVENTION *It is better to prevent waste than to treat or clean up waste after it has been created*	**NO** Waste include NaCl tailings and concentrated brines. E-factor ~2	**YES** No waste or byproduct. Excess water can be recirculated in the system. E-factor ~0
ATOM ECONOMY *Synthetic methods should be designed to maximize incorporation of all materials used in the process into the final product*	**PARTIAL** % Atom Economy = 56% (assuming sylvinite ore is NaCl·KCl)	**YES** % Atom Economy = 100%
LESS HAZARDOUS CHEMICAL SYNTHESIS *Wherever practicable, synthetic methods should be designed to use and generate substances that possess little or no toxicity to human health and the environment*	**NO** Use of frothers such as alkylamines which are generally flammable, toxic and corrosive.	**NO** Use of CaO or $Ca(OH)_2$ which are toxic and corrosive.
DESIGNING SAFER CHEMICALS *Chemical products should be designed to preserve efficacy of function while reducing toxicity*	**PARTIAL** Effect on the total environment of KCl soil applications at fertilization rates not yet fully elucidated	**PARTIAL** Effect on the total environment of hydrothermal material not yet fully elucidated
SAFEST SOLVENTS AND AUXILIARIES *The use of auxiliary substances (e.g., solvents, separation agents, etc.) should be made unnecessary wherever possible and, innocuous when used*	**YES** Solvent is water.	**YES** Solvent is water
DESIGN FOR ENERGY EFFICIENCY *Energy requirements of chemical processes should be recognized for their environmental and economic impacts and should be minimized. If possible, synthetic methods should be conducted at ambient temperature and pressure*	**PARTIAL** Multistep separation process. Requires *T*	**PARTIAL** Two-step process. Requires *T*

USE OF RENEWABLE FEEDSTOCK *A raw material or feedstock should be renewable rather than depleting whenever technically and economically practicable*	**PARTIAL** Evaporitic resources although abundant are not renewable and have a limited geographical distribution	**YES** K-feldspar resources are not renewable but virtually infinite
REDUCE DERIVATIVES *Unnecessary derivatization (use of blocking groups, protection/ deprotection, temporary modification of physical/chemical processes) should be minimized or avoided if possible, because such steps require additional reagents and can generate waste*	**N/A** Principle no applicable	**N/A** Principle no applicable
CATALYSIS *Catalytic reagents (as selective as possible) are superior to stoichiometric reagents*	**N/A** Principle no applicable	**N/A** Principle not applicable
DESIGN FOR DEGRADATION *Chemical products should be designed so that at the end of their function they break down into innocuous degradation products and do not persist in the environment*	**PARTIAL** Long-term fate of chloride ions not fully elucidated	**PARTIAL** Long-term fate of several mineral phases not fully elucidated
REAL-TIME ANALYSIS FOR POLLUTION PREVENTION *Analytical methodologies need to be further developed to allow for real-time, in-process monitoring and control prior to the formation of hazardous substances*	**YES** Process can be monitored to ensure safety and environmental regulations	**YES** Process can be monitored to ensure safety and environmental regulations
INHERENTLY SAFER CHEMISTRY FOR ACCIDENT PREVENTION *Substances and the form of a substance used in a chemical process should be chosen to minimize the potential for chemical accidents, including releases, explosions, and fires*	**NO** Large volumes of highly concentrated hot solutions. Process optimized on processing cost.	**NO** Process operating at *T*, *P* and high pH, similarly to other industrial hydrothermal treatments

4. CONCLUSIONS

Feeding the human population that will inhabit Earth by the year 2050 is a global challenge that requires diverse multidisciplinary research efforts. The effort discussed herein has focused on increasing agricultural yields, especially in those nutrient-poor and scarcely productive soils of the Global South. The cost, availability and efficacy of fertilizers currently used in tropical agricultures need to be addressed, and a reasoned green-chemistry approach may be used to engineer a new generation of affordable and environmentally friendly fertilizers.

Here, we focused on potassium fertilizers (potash), and devised a hydrothermal process according to green-chemistry principles. The hydrothermal material generated after processing exhibits complex mineralogical and chemical properties: i) the particle size distribution spans particles diameters from ~0.1 µm to ~100 µm ii) the constituent mineral phases are altered K-feldspar, hydrogrossular, α-dicalcium silicate hydrate, 11 Å tobermorite, and amorphous calcium-alumino-silicate-hydrate compounds iii) other than hydrogrossular, extensive degree of K incorporation in all mineral phases is observed; traces of carbonaceous species with variable levels of K and Ca are also constituents of the material iv) altered K-feldspar presents Ca-incorporations as a function of the particle size and v) upon leaching, the availability of K, Si, Al and Ca in the hydrothermal material is enhanced with respect to the parent ultrapotassic syenite with K being two orders of magnitude more available than in the rock powder. The preliminary evidence presented in this work suggests that the mechanism for such an enhanced K availability is the hydrothermal alteration of K-feldspar, *i.e.* the hydrolytic dissolution of K-feldspar framework *coupled* with the incorporation of Ca^{2+} in place of K^{+}. Future research will address the characterization of the amorphous phase and the discrimination of the rate of K release from each of the comprising mineral phases.

Preliminary green-chemistry considerations together with the properties of the hydrothermal material indicate a feasible path for introducing a green-chemistry paradigm in potassium fertilization. Raw materials, *i.e.* ultrapotassic syenite, CaO and water are affordable, globally available and compatible with the total environment. Mild processing conditions permit one to envision a relatively easy implementation pathway to industrial scale and may benefit from engineering knowledge available from analogous hydrothermal processes already operating at scale.

5. ACKNOWLEDGEMENTS

Tavarua Invest is acknowledged for funding this research. Dr. Steve Miller (H&M Analytics) is acknowledged for collection of X-ray powder diffraction data and Rietveld refinements. Dr. Benjamin Sabatini is acknowledged for collecting the SEM images reported in Figure 3.

REFERENCES

1 *State of the Tropics*, Cairns, Australia, 2014.

2 W.H. Scherer, K. Konrad, G. Kluge, K. Severin, in *Ullmann's Encyclopedia of Industrial Chemistry*, 2012, pp. 171–197.

3 D. Ciceri, D. A. C. Manning and A. Allanore, *Sci. Total Environ.*, 2015, **502**, 590–601.

4 D. A. C. Manning, *Agron. Sustain. Dev.*, 2010, **30**, 281–294.

5 J. K. Warren, in *Evaporites: A Geological Compendium*, Springer International Publishing Switzerland, 2016, pp. 1081–1185.

6 A. S. R. Juo and K. Franzluebbers, *Tropical soils: properties and management for sustainable agriculture*, Oxford University Press, 2003.

7 D. L. Sparks, *Adv. Soil Sci.*, 1987, **6**, 1–63.

8 V. C. Baligar, N. K. Fageria and Z. L. He, *Commun. Soil Sci. Plant Anal.*, 2001, **32**, 921–950.

9 O. H. Leonardos, W. S. Fyfe and B. I. Kronberg, *Chem. Geol.*, 1987, **60**, 361–370.

10 C. Zorb, M. Senbayram and E. Peiter, *J. Plant Physiol.*, 2014, **171**, 656–669.

11 C. Pieri, R. Oliver. In Proceeding *13th Congress International Potash Institute*, 1986, 73-92.

12 G. Lotz, S. Plitzko, E. Gierke, U. Tittelbach, N. Kersten and W. D. Schneider, *Int. Arch. Occup. Environ. Health*, 2008, **81**, 1003–1019.

13 S. A. Khan, R. L. Mulvaney and T. R. Ellsworth, *Renew. Agric. Food Syst.*, 2014, **29**, 3–27.

14 J. Hollyer, F. Brooks, L. Fernandez-Salvador and L. Castro, *Food Saf. Technol.*, 2013, **56**.

15 H. M. Resh, *Hydroponic Food Production : A Definitive Guidebook for the Advanced Home Gardener and the Commercial Hydroponic Grower*, Boca Raton, FL, 7th edn., 2012.

16 M. E. Lucero, S. Debolt, A. Unc, L. V Reyes and R. L. Mcculley, *Sustain. Agroecosystems Clim. Chang. Mitig.*, 2014, 183–202.

17 *Food Agric. Organ. United Nations*, 2015, 66p.

18 D. Ciceri, M. de Oliveira, R. M. Stokes, T. Skorina and A. Allanore, *Miner. Eng.*, 2017, **102**, 42–57.

19 H. Schultz, G. Bauer, E. Schachl, F. Hagerdon and P. Schmittinger, *Ullmann's Encycl. Ind. Chem.*, 2012, 102.

20 D. A. C. Manning, J. Baptista, M. Sanchez Limon and K. Brandt, *Sci. Total Environ.*, 2017, **574**, 476–481.

21 R.A. Kleiv and M. Thornhill, *Miner. Eng.*, 2007, **20**, 334–341.

22 V.S. Meena, B. R. Maurya and J. P. Verma, *Microbiol. Res.*, 2014, **169**, 337–347.

23 T. Skorina and A. Allanore, *Green Chem.*, 2015, **17**, 2123–2136.

24 S.K. Liu, C. Han, J. M. Liu and H. Li, *RSC Adv.*, 2015, **5**, 93301–93309.

25 X. Ma, J. Yang, H. Ma and C. Liu, *Int. J. Miner. Process.*, 2016, **147**, 10–17.

26 S. Ngqing, M. Hongwen and C. Xiuyun, *Hydrometallurgy*, 2015, **156**, 47–52.

27 M. Hongwen, J. Yang, S. Shuangqing, L. Meitang, Z. Hong, W. Yingbin, Q. Hongbin, P. Zhang and Y. Wengui, *Acta Geol. Sin.*, 2015, **89**, 2058–2071.

28 Y. Zhang, E. Asselin and Z. Li, *J. Chem. Eng. Japan*, 2016, **49**, 111–119.

29 C. Wang, H. Yue, C. Li, B. Liang, J. Zhu and H. Xie, *Ind. Eng. Chem. Res.*, 2014, **53**, 7971–7978.

30 Y. Zhong, J. Gao, P. Chen and Z. Guo, *Energy & Fuels*, 2016, **31**, 699–707.

31 J. Davidovits, *Geopolymer Chemistry & Applications*, Institut Géoplymèr, Saint-Quentin, 4th edn., 2015.

32 C.A. Ríos, C. D. Williams and M. A. Fullen, *Appl. Clay Sci.*, 2009, **43**, 228–237.

33 J.H.P. van Aardt and S. Visser, *Cem. Concr. Res.*, 1977, **7**, 643–648.

34 K. Byrappa and M. Yoshimura, *Handbook of hydrothermal technology*, William Andrew, 2nd edn., 2013.

35 J. Yang, X. M. Tan, H. W. Ma, C. Zeng and H. Peng, *Ferroelectrics*, 2015, **481**, 57–63.

36 *CRC handbook of chemistry and physics*, CRC press, Boca Raton, FL, 97th edn.

37 M. Malmström and S. Banwart, *Geochim. Cosmochim. Acta*, 1997, **61**, 2779–2799.

38 AAVV, *Feldspars and their reactions*, NATO Scien., 1994.

39 S. Brunauer, P. H. Emmett and E. Teller, *J. Am. Chem. Soc.*, 1938, **60**, 309–319.

40 I. G. Richardson, *Cem. Concr. Res.*, 2008, **38**, 137–158.

41 D.A.S. John, A. W. Poole and I. Sims, *Concrete petrography. A handbook of investigative techniques*, Arnold, 1998.

42 B.S. Tubaña and J. R. Heckman, in *Silicon and Plant Diseases*, Springer International Publishing, 2015, pp. 7–51.

43 Ralph K. Iler, *The chemistry of silica*, A Wiley-Interscience publication, 1979.

44 W.A. Deer, R.A. Howie and J. Zussman, *Framework Silicates. Feldspars*, The Geological Society, London, 2nd edn., 2001.

45 M. Lagache, in *Feldspars and Feldspathoids*, ed. W. L. Brown, Springer-Science+Business Media, B.V., Dordrecht, Holland, 1984, pp. 247–279.

46 Shuangqing S., Ma H., Chuan X. *Hydrometallurgy*, 2015, **156**, 47-52.

47 S. Fujita, S. Kenzi and Y. Shibasaki, *J. Mater. Cycles Waste Manag.*, 2002, **4**, 41–45.

48 H. Maeda, Y. Kurosaki, T. Nakamura, M. Nakayama, E. H. Ishida and T. Kasuga, *Mater. Lett.*, 2014, **131**, 132–134.

49 H. Ishida, S. Yamazaki, K. Sasaki and Y. Okada, *J. Am. Chem. Soc.*, 1993, **76**, 1707–1712.

50 H. Taylor, *Cement Chemistry*, Thomas Telford Publishing, 2nd edn., 1997.

51 J.R. Houston, R. S. Maxwell and S. A. Carroll, *Geochem. Trans.*, 2009, **10**, 1.

52 O. Watanabe, K. Kitamura, H. Maenami and H. Ishida, *J. Am. Ceram. Soc.*, 2001, **22**, 2318–2322.

53 S. Shaw, S. M. Clark and C. M. B. Henderson, *Chem. Geol.*, 2000, **167**, 129–140.

54 L. Galvánková, J. Másilko, T. Solný and E. Štěpánková, *Procedia Eng.*, 2016, **151**, 100–107.

55 N. Bell S., S. Vinigalla, P. Gill M. and A. H. James, *J. Am. Ceram. Soc.*, 1996, **79**, 2175–2178.

56 H. Sato and M. Grutzeck, *Mater. Res. Soc. Symp. Proc.*, 1992, **245**, 235–240.

57 S. Komarneni, *Science*, 1983, **221**, 647–648.

58 S. Komarneni, E. Breval, M. Miyake and R. Roy, *Clays Clay Miner.*, 1987, **35**, 385–390.

59 C. Biagioni, S. Merlino and E. Bonaccorsi, *Mineral. Mag.*, 2015, **79**, 485–495.

60 J.H.P. van Aardt and S. Visser, *Cem. Concr. Res.*, 1977, **7**, 39–44.

61 L. L. Stillings, S. L. Brantley and M. L. Machesky, *Geochim. Cosmochim. Acta*, 1995, **59**, 1473–1482.

62 Ciceri D., Allanore A. *PloS one*, 2015, **10.10**, e0139979.

ELECTRONIC SUPPLEMENTARY INFORMATION (ESI)

GREEN-CHEMISTRY SYNTHESIS OF POTASSIUM FERTILIZER VIA HYDROTHERMAL ALTERATION OF K-FELDSPAR ORE

Davide Ciceri[a], Marcelo de Oliveira[a], Antoine Allanore[a]

[a] Department of Materials Science and Engineering, Massachusetts Institute of Technology, Cambridge MA 02139, USA

ESI 1. PRELIMINARY CONSIDERATIONS ON GREENHOUSE GASES EMISSIONS DERIVING FROM TRANSPORT OF POTASH

A preliminary model is proposed to assess CO_2e emissions due to transport of 1 ton of K_2O from the mines located in Saskatchewan, Canada, to the Cerrado region, Brazil.

It is assumed that a ton of KCl travels:

- A total of 1,600 km by diesel-powered train within Canada, corresponding to the distance between potash mines in Saskatchewan and the port of Vancouver in British Columbia[§].
- A total of 15,729 km (~8,493 nautical miles – 35 days journey) by ocean cargo ship, corresponding to the distance from the port of Vancouver and Port of Santos, São Paulo State, Brazil[‡].
- A total of 2,100 km by truck within Brazil, corresponding to the distance between Port of Santos and Sinop, which is the major agricultural center in the State of Mato Grosso[†].

CO_2e emissions are calculated according to emission factors under two different hypothesis.

- **First hypothesis**

  This hypothesis is based on tabulated values of CO_2e emission as a function of the type of transport used:
  - Transport on Canadian rail[‡]: 0.01785 kg CO_2e t^{-1} km^{-1}
  - Transport on panamax bulk carrier[1]: 0.00536 kg CO_2e t^{-1} km^{-1}
  - Transport on truck (assumed for Brazil to have the same emission factors as in the EU for bulk goods moved on a 24-40 t GCW lorry)[2]: 0.065 kg CO_2e t^{-1} km^{-1}

Under this first hypothesis, the total CO_2e emissions due to transport are 249 kg CO_2e t^{-1}. Assuming that a ton of KCl fertilizer is equivalent to 0.61 t of K_2O, then the equivalent emissions due to transport are 409 kg CO_2e t^{-1}_{K2O}.

- **Second hypothesis**

  This hypothesis is based on tabulated values for fuel consumption and Well-To-Wheel (WTW) CO_2e emission factors, both according to the Global Logistics Emission Council (GLEC)[3].
  - Fuel consumption on train powered by Heavy Fuel Oil (HFO) is 0.005 kg_{fuel} t^{-1} km^{-1} (regional value for North America) at emission factor of 3.42 kg CO_2e kg^{-1}_{fuel} (global value)

---

§ http://www.canpotex.com/what-we-do/logistics

‡ seadistances.org

† Google Maps, Departamento Nacional de Estradas de Rodagem (Brazil)

‡ https://www.cn.ca/en/repository/popups/ghg/ghgcalculatoremissionfactors

- Fuel consumption on container ship powered by Heavy Fuel Oil (HFO) is 0.006 kg_{fuel} t^{-1} km^{-1} (global value) at emission factor of 3.42 kg CO_2e kg^{-1}_{fuel} (global value)
- Fuel consumption on 40t/Class 8 ambient temperature truck by diesel is 0.023 kg_{fuel} t^{-1} km^{-1} (EU value) at emission factor of 3.90 kg CO_2e kg^{-1}_{fuel} (EU value)

Under this second hypothesis, the total CO_2e emissions due to transport are 539 kg CO_2e t^{-1}. Assuming that a ton of KCl fertilizer is equivalent to 0.61 t of K_2O, then the equivalent emissions due to transport are 883 kg CO_2e t^{-1}_{K2O}.

In 2014, Brazil imported 5,291,619 tons of agricultural K_2O[4]. Under the present assumptions and uncertainties, this would correspond to emissions in the order of 2.2Mt CO_2e (first hypothesis) and 4.7Mt CO_2e (second hypothesis). As a term of comparison, the total equivalent emissions due to the entirety[§] of agricultural activities in Brazil corresponded for the same year to 44.2 Mt of CO_2e [4]. Therefore, in Brazil, transport of K_2O alone is comparable to 4.9% to 10.6% of the total agricultural emissions.

[§] CO_2e emissions due to transport of the fertilizers are not included in the total CO_2e emissions

Table ESI 1 Overview of hydrothermal reactivity of CaO-Al_2O_3-SiO_2-H_2O systems.

Reagents	**molar ratios**		***T***	***t***	**solvent**	***S*:*L***	**stirring**	**phases observed**[B]	**reference**
	Al/(Si+Al)	Ca/(Si+Al)	°C	h	-	weight ratio[A]	-	-	-
$Ca(OH)_2$ SiO_2 gel γ-Al_2O_3 (amorphous)	0.67	1.00	150	6	water + KOH	1:10	n/a	$Ca(OH)_2$ hydrogrossular $CaCO_3$	5
CaO SiO_2 (amorphous) Al_2O_3 (amorphous)	0.15	0.83	150	0-190	water + NaOH	1:10; 1:5	N	C-S-H 11 Å tobermorite	6
CaO coal ash $Al(OH)_3$ or Al_2O_3 (sol)	0.57	0.86	100-180	15	water	1:6	Y	hydrogrossular 11 Å tobermorite $CaCO_3$	7
CaO (meta)kaolinite SiO_2 (precipitated) Al_2O_3	0.10-0.13	6.50-1.00	175	0.5-24	water	2:1	N	quartz $Ca(OH)_2$ C-S-H; α-C_2SH 11 Å tobermorite $CaCO_3$	8
K-feldspar	0.25	0.22	190-220	20	water + NaOH water + KOH water + $Ca(OH)_2$	1:6	N	altered K-feldspar hydrogrossular C-S-H; C-A-S-H; α-C_2SH tobermorite $CaCO_3$; K_2CO_3; $K_2Ca(CO_3)_2$	9
$Ca(OH)_2$ Ultrapotassic syenite	0.24	0.17	200	5	water	1:4	Y	altered K-feldspar hydrogrossular C-A-S-H; α-C_2SH 11 Å tobermorite unidentified carbonates	This study

[A] Assumes a density of 1 g mL^{-1} for all solutions. Values are rounded.

[B] C-A-S-H=non-stoichiometric calcium aluminum silicate hydrate; C-S-H=non-stoichiometric calcium silicate hydrate; α-C_2SH=α-dicalcium silicate hydrate

ESI 2. CALCIUM OXIDE (CaO) CHARACTERIZATION

Despite a controlled storage system, the CaO used in this study (reagent grade, Alfa Aesar) was subjected to a high degree of hydration. An XRPD scan showed that the actual composition at the time of the experiment was the following: CaO 5.5 wt%, $Ca(OH)_2$ 93.7 wt%, $CaCO_3$ 0.8 wt%.

According to the manufacturer, the level of impurities in the material as received is as follow:

- 0.005% Cl max
- 0.05% NO_3 max
- 0.1% Fe max
- 0.1% SO_4 max
- Insoluble material: 1.5% max in CH_3COOH and NH_4OH

Trace Metals: (as Pb) 0.01% max

ESI 3. SCHEMATIC OF THE HYDROTHERMAL REACTOR

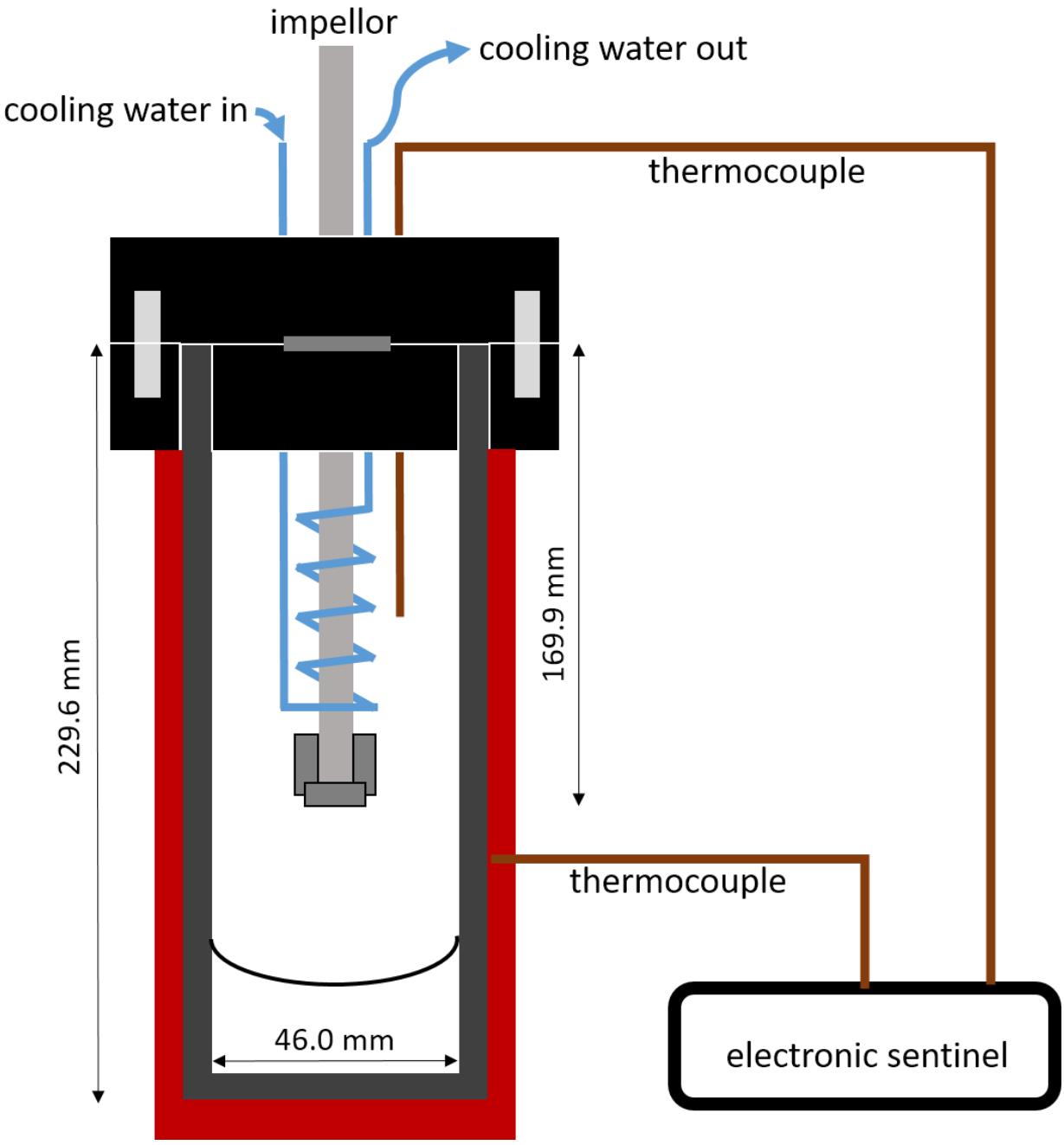

Figure ESI 1 Schematic representation of the hydrothermal reactor used in the present study (Parker, EZE-Seal®, 300 mL). The jacket outside the reactor (depicted in red) is a ceramic heating mantle.

ESI 4. TEMPERATURE AND PRESSURE VARIATION DURING THE SYNTHESIS OF THE HYDROTHERMAL MATERIAL

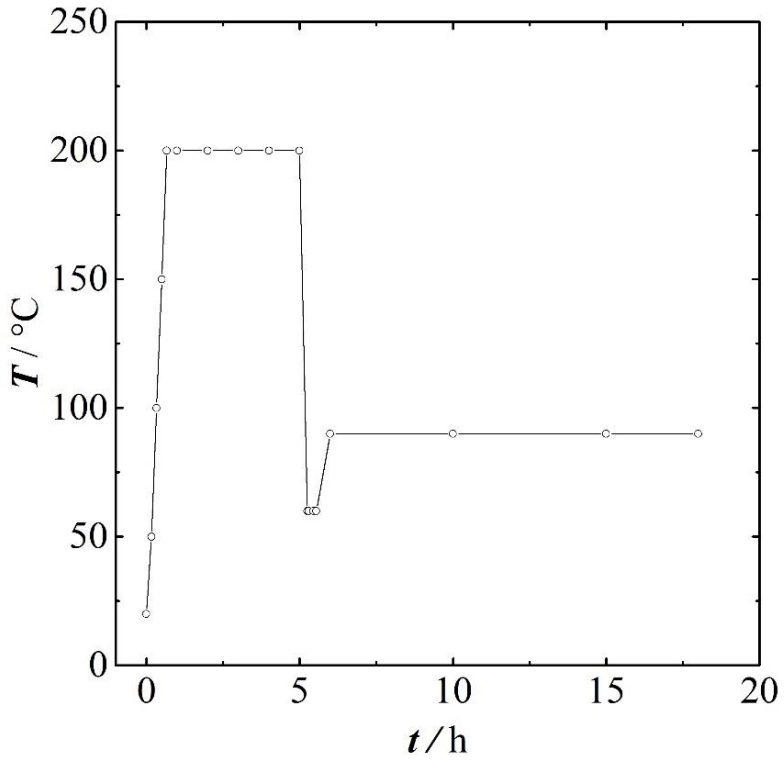

Figure ESI 2 Temperature profile during the processing steps that lead to the hydrothermal material.

ESI 5. APPEARANCE OF THE HYDROTHERMAL MATERIAL

Figure ESI 3 Photographs illustrating the physical appearance of ultrapotassic syenite rock powder (left) and hydrothermal material (right). Both samples showed here are ~2 g. A much more loose packing and possibly a lower density are observed for the hydrothermal material rather than for the ultrapotassic syenite. Actual density measurements were not performed.

ESI 6. CHANGE IN pH DURING LEACHING EXPERIMENTS

Figure ESI 4 shows the variation in pH of a solution of HNO_3 at initial nominal pH=5 upon contact with either the ultrapotassic syenite or the corresponding hydrothermal material. A calibrated pH meter (Hanna, HI 4222) is probing in a beaker the pH of the HNO_3 solution at pH=5 for 5 min, after which a mass of ultrapotassic syenite or hydrothermal material is added under agitation at m_S:m_L=0.1, simulating the conditions of the leaching test. Within a few minutes, the pH of the solution raise to a nominal value of ~6 units in the case of the rock powder, and ~12 units in the case of the hydrothermal material. The system is reactive and the pH never reaches a true chemical equilibrium. In the rock powder as well as in the hydrothermal material, the dissolution of the K-feldspar component alone proceeds indefinetively, until complete tranformation on geological timescales occur. Such processes change the pH of the leaching environment over time.

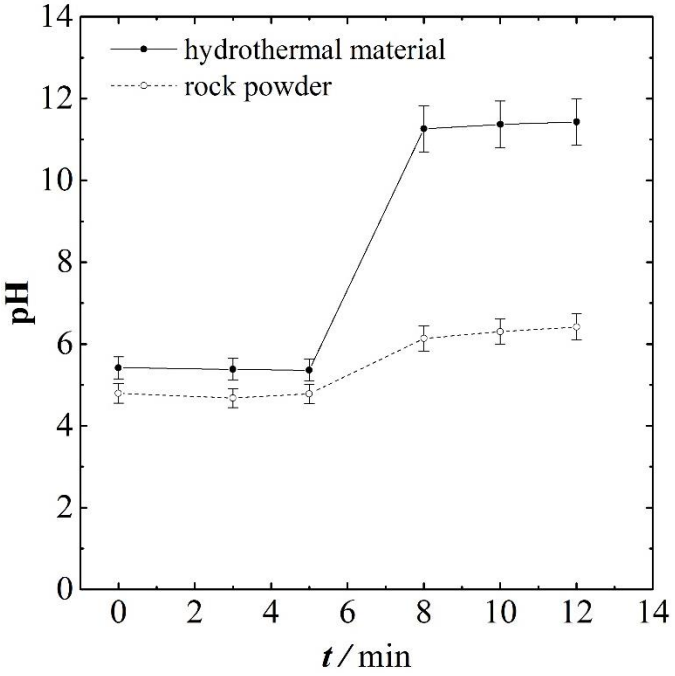

Figure ESI 4 Spontaneous variation of the pH of a solution of HNO_3 at an initial nominal pH=5 contacted with either the rock powder (ultrapotassic syenite) or the hydrothermal material at a m_S:m_L=0.1 and room temperature. The solid is maintained agitated with a magnetic stirrer. Error bars show an arbitrary error of 5%.

ESI 7. X-RAY POWDER DIFFRACTION PATTERN

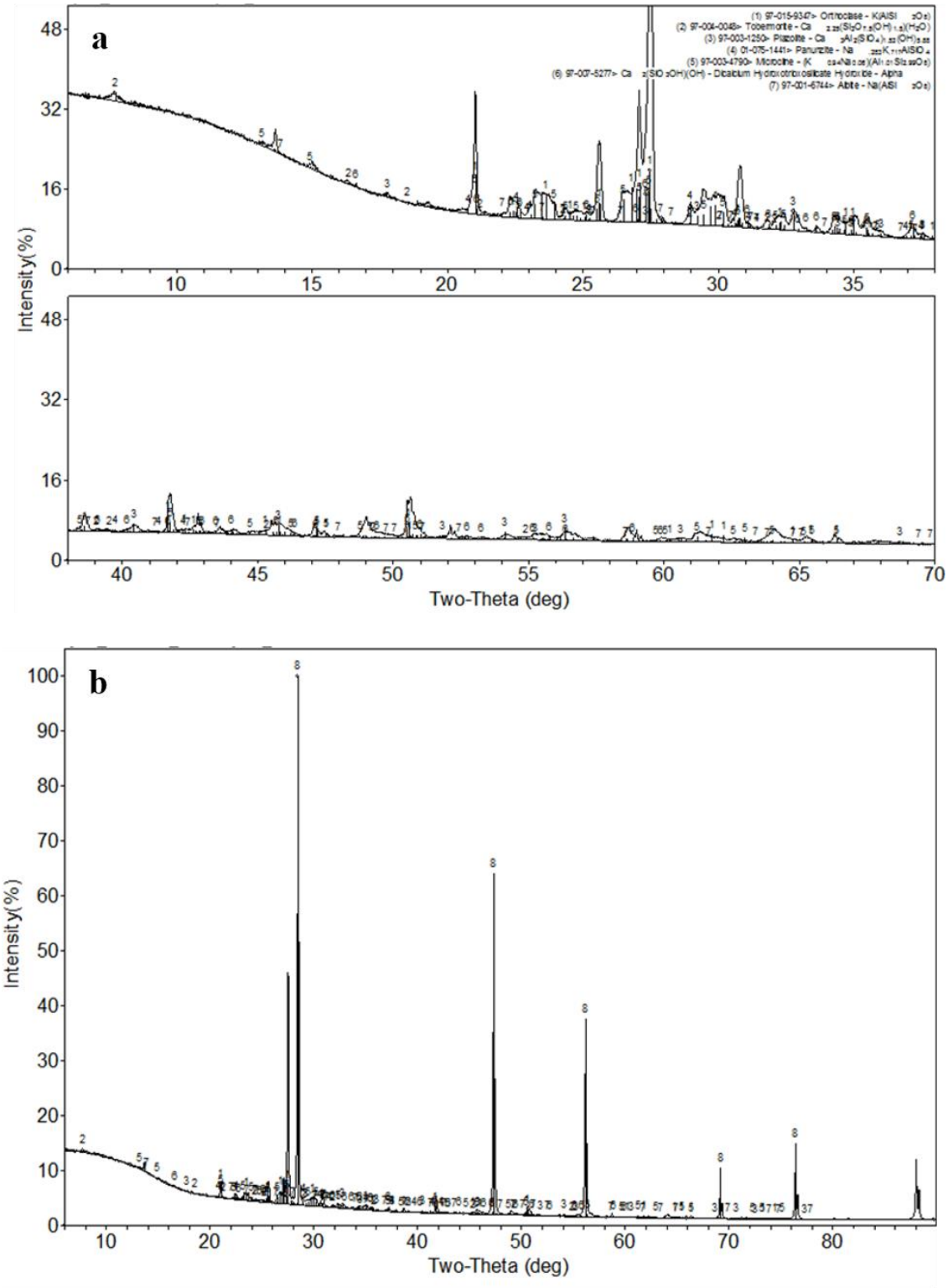

Figure ESI 5 XRPD pattern of (a) sample of hydrothermal material as such and (b) sample spiked with 50 wt% of Si (NIST SRM 640) for determination of the amorphous component. Inorganic Crystal Structure Database (ICSD) numbers are as follow: orthoclase (#159347); microcline (#34790); plazolite (#31250); α-dicalcium silicate hydrate (#75277); 11 Å tobermorite (#40048); albite (#16744); panunzite (#30951).

ESI 8. OVERVIEW OF SEM MICROGRAPHS OF THE HYDROTHERMAL MATERIAL

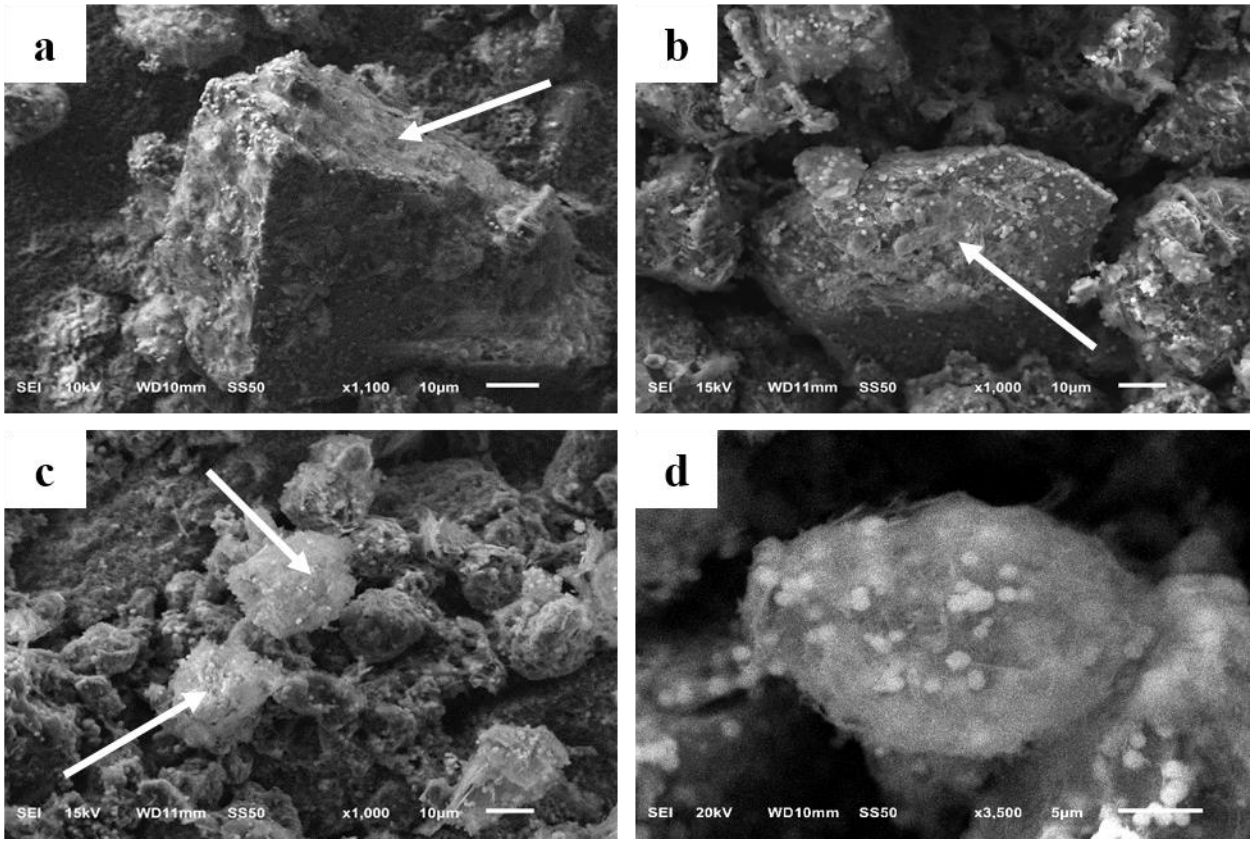

Figure ESI 6 Overview of the hydrothermal material (powder): (a) and (b) altered K-feldspar; round particles of hydrogrossular are clearly visible; the white arrow points at a side of the feldspar surface where fine needles of calcium silicate phases are particularly evident as a moss-like coating (c) white arrows point at round agglomerates (presumably tobermorite); cross sections of such formations are likely to resemble those highlighted in Figure 3b and Figure 3d of the main text (d) close up of one of those formation shown in (c); round particles of hydrogrossular are clearly visible. Images were obtained by dusting a pinch of powder on conductive paint (Carbon Conductive Adhesive 502, Electron Microscopy Sciences).

ESI 9. ELECTRON PROBE MICRO-ANALYZER (EPMA) CHARACTERIZATION OF ULTRAPOTASSIC SYENITE, FEED MIXTURE AND HYDROTHERMAL MATERIAL

An EPMA study was performed on the rock as such, the feed mixture and the hydrothermal material, to understand if ball milling may lead to inclusion of Ca atoms in the feldspar structure. The EPMA experimental protocol was the same described in the main text. All samples are mounted in thin section.

- **Ultrapotassic syenite (thin section)**

Results for MCA41 rock mounted in thin section are reported in ESI-EPMA. The average K_2O content from point analysis was 14.9 wt%, which is in good agreement with the value determined by XRF on the same rock ground in a ball mill (14.3 wt%)[10]. In the feldspar structure of the rock, no Ca was detected, and the total content of oxides neared 100%.

- **Feed mixture**

Results for the feed mixture mounted in thin section are reported in ESI-EPMA. For some of the smallest particles, K-feldspar was enriched in Ca, depleted in K, Si and Al. In general, such an observation does not seem to hold true for bigger K-feldspar grains (> 50 μm). Such findings can be explained according to at least three different hypothesis: i) the Ca detected by EPMA is native to the ultrapotassic syenites; such domains enriched in Ca may break up more easily upon milling, and therefore they are consistently detected in the particles <50 μm. This hypothesis is unlikely given the results discussed above for the rock in thin section. However, note that ball milling has been proved to affect the crystallinity, and possibly also the composition of ultrapotassic syenites as a function of the particles size fraction[5] ii) the energy input during ball milling may activate via mechanical action a process of Ca insertion in K-feldspar iii) Ca is coating the K-feldspar grains, but is not inserted in the crystalline framework. Most likely, a combination of phenomena is actually occurring, and it will be the subject of future investigations.

- **Hydrothermal material**

Selected X-ray elemental maps of the hydrothermal material obtained with EPMA are shown in Figure ESI 7. Specifically, Figure ESI 7(a-c) shows three particles of K-feldspar in three diferent size classes. The small grain is highly depleted in K and enriched in Ca. Al and Si also seem to be particularly depleted with respect to pristine K-feldspar in ultrapotassic syenites. As the particles become bigger such chemical alteration becomes less evident, although a rim of calcium minerals is observed consistently. Note that elemental maps cannot be looked at independently from point analysis (ESI-EPMA). Figure ESI 7(d-f) shows additional selected particles commented in caption.

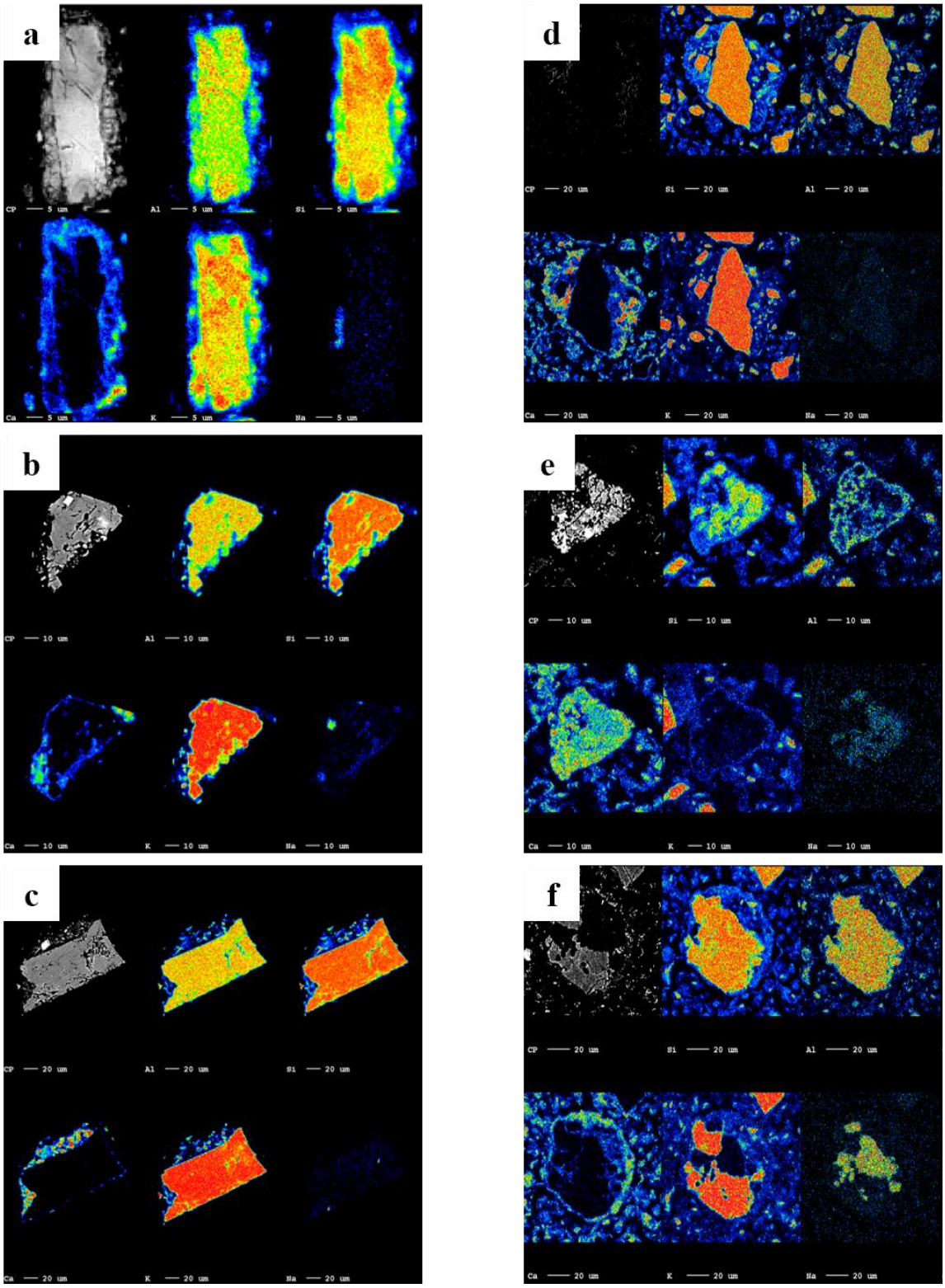

Figure ES1 7 Electron Probe Micro-Analzer (EPMA) X-ray elemental maps. (a) (b) (c) particles of altered K-feldspar in three different size classes, *d*<50µm, 50<*d*<100µm and *d*>100µm, respectively; (d) clump-like formation in the hydrothermal material (compare with Figure 3d of the main text); large mass of hydrogrossular (compare with Figure 3d of the main text); (f) clump-like formation with the central particle of altered K-feldspar containing a distinct inclusion of albite.

ESI 10. ACID-BASE TITRATION OF HYDROTHERMAL MATERIAL

An acid-base titration of the hydrothermal material was carried out as follow:

- First, 0.3 g of hydrothermal material were suspended in 10 mL of DI water under agitation
- Second, standardized 0.1 M HNO_3 (Alfa Aesar) was added to the beaker. After each acid addition (2.5 mL), the system was let to stabilize for 15 min, before the reading was taken. Note that the pH never truly stabilized due to surface reactivity
- Third, the titration curve is plotted as shown in Figure ESI 6, and equivalent points used for back calculations of the base content in the hydrothermal material.

Two distinct equivalent points are observed, at pH=10.0 (3.0 mL) and pH=5.8 (12.0 mL). The first equivalent point can be reasonably attributed to carbonates since the tabulated pKa_2 value for H_2CO_3 is 10.33 (25°C). Differences between experimental and theoretical values may be explained by interferences caused by the surface reactivity of the other mineral phases such as K-feldspar, hydrogrossular and tobermorite. The second equivalent point seems farer from the tabulated pKa_1 value for H_2CO_3, which is 6.35 (25°C). Assuming the first equivalent point is indeed due to carbonates, this would correspond to 0.3 mmol of CO_3^{2-}, equivalent to 4.3 wt% of CO_2 in the hydrothermal material. Such an amount was not detected by XRPD, but is in excellent agreement with LOI data (Section 2.2. of the main text). Carbonates were anhedral crystals, but not amorphous, and are not detected by XRPD likely because they are below detection limit. If all of the carbonate determined with the titration at the first equivalent point was K_2CO_3, then the expected K leaching test would be 78,000 ppm_K, well-above the experimental data (Figure 5 of the main text). Carbonates in the hydrothermal material are therefore an unidentified mixture, which is likely to comprise K_2CO_3, Na_2CO_3, $MgCO_3$, $CaCO_3$, but possibly also other double carbonate species such as $K_2Ca(CO_3)_2$ (bütschiilite and/or fairchildite)[11]. The second equivalent point does not match the content of carbonate detected at the first equivalent point. Assuming that the second equivalent point is due to the equilibrium $HCO_3^- + H^+ \rightleftharpoons H_2CO_3$, then further to the 0.3 mmol of CO_3^{2-} additional 0.6 mmol of bicarbonate species HCO_3^- must be present originally in the hydrothermal material. Such an amount would correspond to an additional 8.6 wt% of CO_2 content in the hydrothermal material, for a total of 12.9 wt% of CO_2, which is unlikely to be undetected by XRPD. We are not able to discriminate if such discrepancies are due to analytical error during titration, analytical error during XRPD collection, multitude of carbonaceous species that are all below or near detection limits or strong interference in the titration from other mineral components. Despite such limitations, data point to an effective presence of carbonates in the hydrothermal material.

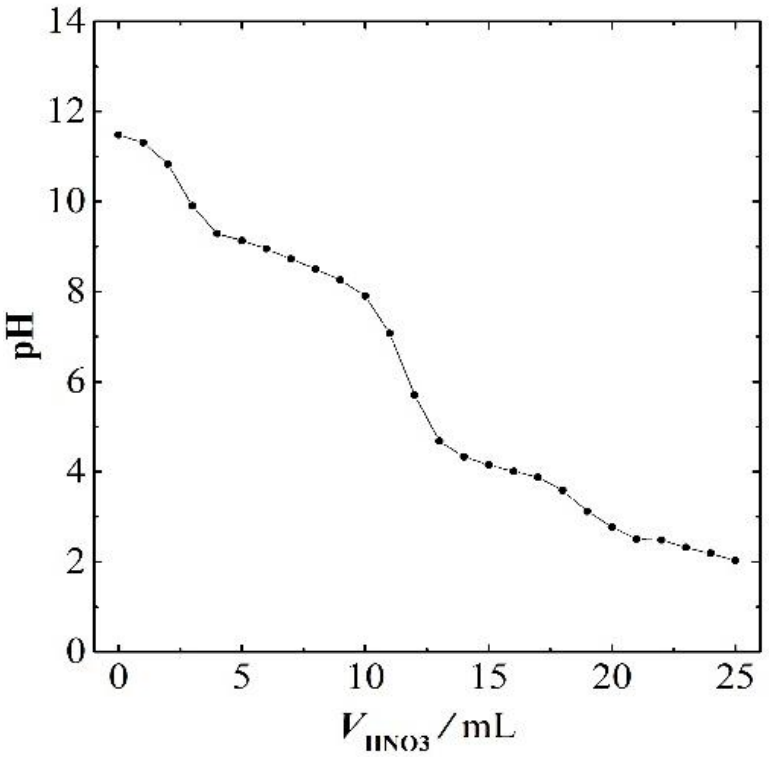

Figure ESI 8 Titration curve of the hydrothermal material (0.3067g) suspended in 25 mL of DI water, with standardized HNO_3 0.1 M (Alfa Aesar).

ESI 11. QUALITATIVE SPOT TEST FOR THE DETERMINATION OF CARBONATES

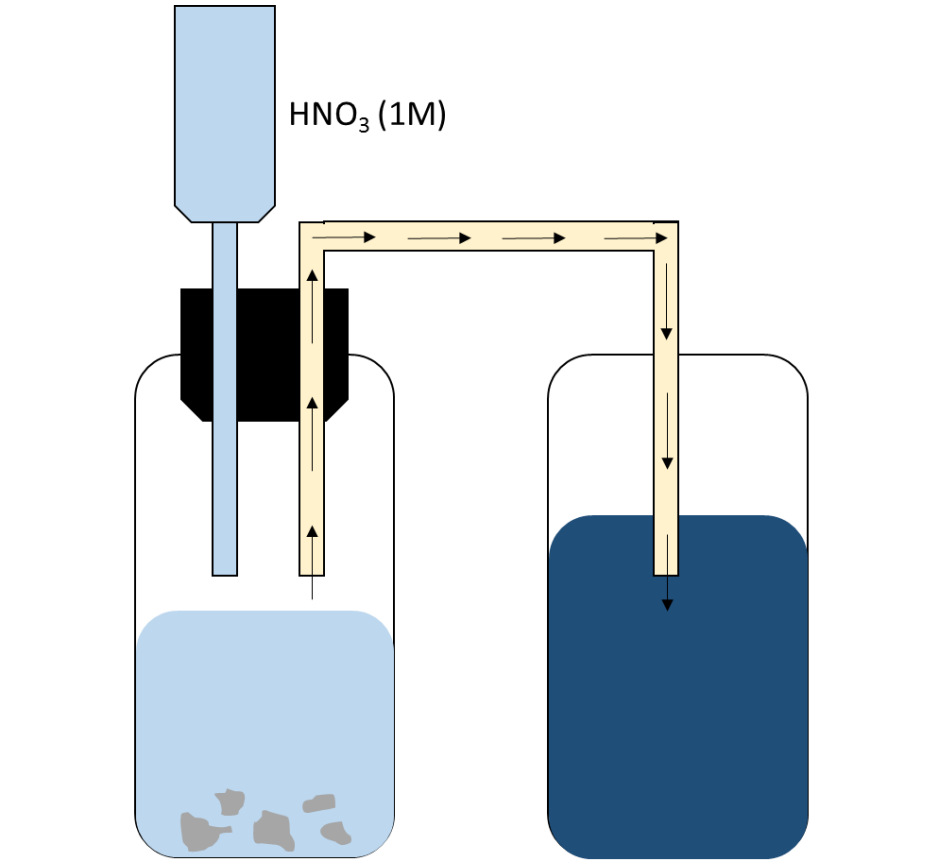

(a)

(b)

(c)

Figure ESI 9 Spot test for the determination of carbonates in the hydrothermal material. (a) Schematic and principle of the experimental apparatus. Concentrated nitric acid (15.6 M) is dropped on top of the material. If carbonates are present, they generate CO_2, which is channeled into a second compartment of the apparatus and precipitated as $BaCO_3$ from a solution of $Ba(OH)_2$ (b) result from a blank test, where the material is ultrapotassic syenite (no $BaCO_3$ is formed) (c) result from a test with the hydrothermal material. A whitish cloud of $BaCO_3$ is formed, confirming the presence of carbonates.

ESI 12. N_2 ADSORPTION/DESORPTION ISOTHERM OF THE HYDROTHERMAL MATERIAL

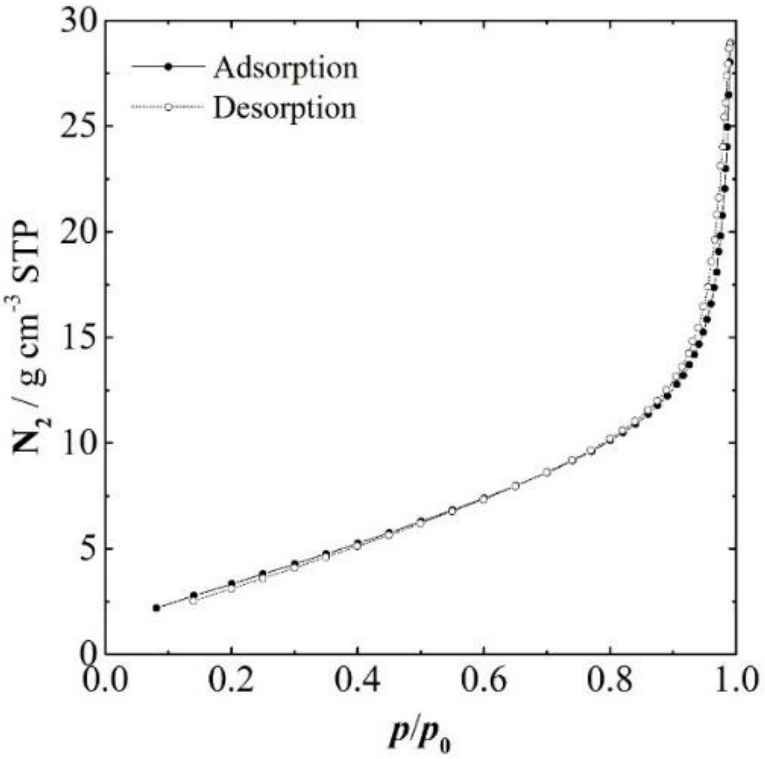

Figure ESI 10 Adsorption and desorption isotherms (-196°C) of N_2 gas at the surface of the hydrothermal material.

ESI 13. MASS BALANCE CONSIDERATIONS

Table ESI2 Overview of data used for mass balance calculations

	K-feldspar (wt %)	K_2O (wt %)	H_2O (wt %)	MM (g/mol)
Ultrapotassic syenite	94.5	14.3	0.1	n/a
K-feldspar	n/a	14.9±0.3	0.0	278.3
Hydrothermal material	66.5	11.7	4.4	n/a
K	n/a	n/a	n/a	39.1
K_2O	n/a	n/a	n/a	94.2

The potassium mass balance was calculated using the data in Table ESI2, as follow:

- Feed mixture:
    - 21.28 g of ultrapotassic syenite + 3.72 g of CaO
    - K-feldspar equivalent: 20.11 g
    - K equivalent: 2.49 g
    - K_2O equivalent: 3.00 g
- Hydrothermal material:
    - Total mass is 26.1 g
    - K-feldspar equivalent: 17.3 g (measured by XRPD; see main text)
    - K-feldspar consumed: 2.8 g or ~16% (equivalent to 0.4 g of K or 0.5 g K_2O)
- Leaching:

  Assume that all K contained in the K-feldspar that was completely converted is fully available in the leaching test. Furthermore, assume that the K available from the remaining altered K-feldspar is negligible. This is justified by considering that the dissolution rate of K-feldspar at pH=12 (ESI S6) reported by Blum[12] is 5.6×10^{-12} mol m^{-2} s^{-1}, corresponding to a range 12.6-189.0 ppm of available K[1].

  Then:
    - Leaching forecast: 15,126±1,976 ppm K (assuming a 1.5% error on XRPD)
    - Leaching experimental: 14,065±744 ppm_K, which is within 7% of the calculated value

[1] A specific surface area of 1 or 15 g m^{-2} is assumed for the K-feldspar fraction in the hydrothermal material.

REFERENCES

1 *Minist. Ecol. Sustain. Dev. Energy. French Repub.*, 2012.

2 *Eur. Assoc. Forwarding, Transp. Logist. Cust. Serv.*, 2012.

3 *Smart Freight Centre, 2016. GLEC Framework for Logistics Emissions Methodologies*, Version 1.0. Available from www.smartfreightcentre.org.

4 *Food and Agriculture Organization of the United Nations.*, 2016. FAOSTAT statistics database. Rome.

5 H. Maeda, Y. Kurosaki, T. Nakamura, M. Nakayama, E. H. Ishida and T. Kasuga, *Mater. Lett.*, 2014, **131**, 132–134.

6 J.R. Houston, R. S. Maxwell and S. A. Carroll, *Geochem. Trans.*, 2009, **10**, 1.

7 S. Fujita, S. Kenzi and Y. Shibasaki, *J. Mater. Cycles Waste Manag.*, 2002, **4**, 41–45.

8 C.A. Ríos, C. D. Williams and M. A. Fullen, *Appl. Clay Sci.*, 2009, **43**, 228–237.

9 S.K. Liu, C. Han, J. M. Liu and H. Li, *RSC Adv.*, 2015, **5**, 93301–93309.

10 D. Ciceri, M. de Oliveira, R. M. Stokes, T. Skorina and A. Allanore, *Miner. Eng.*, 2017, **102**, 42–57.

11 S. K. Liu, C. Han, J. M. Liu and H. Li, *RSC Adv.*, 2015, **5**, 93301–93309.

12 A. E. Blum, in *Feldspars and their reactions*, Kluwer Academic Publishers, 1st edn., 1994, pp. 595–630.